Department of Electrical
and
Computer Systems Engineering

Technical Report
MECSE-27-2004

Design of Photonic Half-band Filters Using Multirate DSP Technique

LN Binh and VAT Tran

MONASH
UNIVERSITY

DESIGN OF PHOTONIC HALF-BAND FILTERS USING DIGITAL SIGNAL PROCESSING TECHNIQUE

L. N. Binh and V.A.T. Tran

Department of Electrical and Computer Systems Engineering

Monash University, Clayton Victoria 3168 Australia

e-mail le.nguyen.binh@eng.monash.edu.au

ABSTRACT

Photonic filters are very important in advanced DWDM optical communications systems as they are capable to select certain wavelength or group of wavelength channels or filter certain optical frequency band of modulated signals. Half band filters thus form an important class of zero-phase type and would find important applications in generation of advanced modulation formats optical transmission systems. In this paper, the generic characteristics of optical filter and synthesis of the band-pass optical filters (OF) are described. The design of optical half band filters (HBF) is given using the photonic signal processing technique and the graphical optical circuit epresentation. Their photonic circuit configurations and characteristics are identified and compred with specific properties of the finite-impulse response (FIR) and the infinite-impulse response (IIR) half-band filters (HBFs). Multi-rate digital signal processing is employed to achieve different sampling rates and hence superposition of different passband regions to form the desired band at different stages is described for the synthesis of optical band-pass filters. The characteristics and circuit configurations of optical FIR HBFs, IIR HBFs are proposed. The photonic signal flow graph (SFG) method is used to obtain the transfer functions between any two nodes of a phonic circuit.

The effects of the passband and cut-off band characteristics of Butterworth and Chebyshev optical band-pass filters on the 40 Gb/s optical carrier modulated signals using various modulation formats such as DSB (Double Sideband), VSB CS-RZ (Vestigial Sideband Carrier-

suppressed Return-to-Zero) are also investigated for optical transmission systems. The VSB CS-RZ offers better spectral efficiency as compared to the DSB format.

Furthermore the characteristics of the CS-RZ format is proved to be more attractive and resilient than any other formats such as RZ (Return-to-Zero) and NRZ (Non-Return-to-Zero) formats as is much more tolerant to nonlinear effects, especially when DWDM is used in which several optical channels are multiplexed and transmitted over a single fibre. High spectral efficiency of the VSB CS-RZ format is suitable for the high channel bit rate 40 Gt/s over ultra-long transmission distance. This work will reported in the next part of the technical report.

TABLE OF CONTENTS

1 Introduction

Photonic filters are very important for optical communications systems and photonic signal processing [1]. Optical resonance filterscan be considered as a form of sharp narrow band OFs are often used in practical systems [2] . They can be employed as frequency - selective devices, tuneable filters [**3**]; or narrowband division multiplexers [**4**]; even as optical equalizers [**5**] in high – speed transmission systems [**6**]. Optical resonance filters could be implemented using 4-port optical directional couplers [**7**], [**8**]. These photonic circuits are quite simple [**9**], adjustable [**4**] since a simple-ring resonator can be obtained by looping one of the output ports of a 4-port directional coupler back to the input port [**10**]. OFs using optical directional couplers are very practical due to their ease of applications. On the other hand HBFs are cascades of individual filters each with different centre passband that could be designed to form any desired phase and amplitude responses.

Recently multi-terabit transmissions with 40 Gb/s per channels with moderate spectral efficiency have been reported [**11**]. Multi-terabit transmission experiments have been investigated and a different techniques have been developed. It is desirable that 40 Gb/s systems should have the same amplifier span spacing as the existing 10 Gb/s systems. The main issues are the distortion and non-linearity optical effects in transmission fiber. In particular, Self-Phase-Modulation (SPM), resulting from fiber non-linearity caused by Group Velocity Dispersion (GVD), leads to waveform distortion that limits the maximum transmission distance and capacity of high-speed optical links. Modulation formats such as the Return-to-Zero (RZ) format, Non-Return-to-Zero (NRZ) format, Carrier-Suppressed Return-to-Zero (CS-RZ) format etc. can be exploited with their properties of narrower bandwidth, lower carrier power to reduce the nonlinear effects and linear dispersion of ultra-long haul and ultra-high bit rate optical transmission systems. RZ format has been proven to be more robust against the waveform dispersion induced by SPM and

GVD interaction than the NRZ format [**12**]. CS-RZ format was suitable format for optical transmission at 40Gbps with 0.8bit/s/Hz spectral efficiency [**13**].

As often used in multi-rate digital signal processing, optical HBFs can offer its excellent property in the asymmetry of its passband and hence efficient filtering of half of the optical band for vestigial single side band format. As investigated in early 2000, Jinguji *et al* [**14**] reported a very interesting design of HBFs that used optical delay-line circuits which might be converted to optical resonator configurations [**9**]. Although linear phase of FIR HBFs have attracted much interests [**15**]. The design technique for equip-ripple optical HBFs had not been investigated for optical filters. Both optical FIR and IIR HBFs are important for these OFs [**15**].

In generic term FIR HBFs can be understood as optical all-pass filters where all poles of the systems located at the origin. On the other hands, optical IIR HBFs having all poles and zeros located else where, not at the origin. Ref. [**14**] presented the optical transfer characteristics in matrix forms where only odd order systems could be observed. The characteristics of a system stated in matrix form are general and simple. However, we have devised the photonic SFG technique that would simplify the derivation of any optical transfer function from any two nodes of a photonic circuit or network of circuits. The SFG technique [**16**] and particularly the Manson's rule has been proven very powerful for such applications. This is presented in the next section. Indeed the SFG method had been known in control systems where the given block diagrams are set [**17**], and also available in electrical-electronic circuits [**18**].

Given the significant needs in this optical field, the main aim of this paper is to detail the design techniques for photonic filters and its applications in transmission of ultra-high bit rate signals, especially at 40 Gbps/channel. Further, multi-rate digital signal processing discrete systems are applied to synthesise the HBF characteristics. The specific objectives of this work are described as follows. (i) To obtain a synthesis technique for OFs incorporating optical resonance circuits. Photonic SFG is developed and the photonic Manson's rule is developed in order to simplify the derivation of the optical transfer function or transmittance of complex photonic systems or

circuits . The design of optical band-pass Butterworth/Chebyshev filters is illustrated. (ii) To integrate the HBFs for generation of VSB signals in 40Gbps/channel transmission system. and (iii) To investigate the sensitivity of pass-band and stop-band frequencies of the HBF especially the locations of the poles and zeros of the filter transfer function are studied to achieve certain pass band characteristics.

The paper is organized as follows: Section 2 introduces the design technique based on the optical SFG technique for OF, as well as some introductory remarks on several types of modulation-formats; Section 3 gives an introduction on optical resonators, optical HBFs and their applications in DWDM optical communications systems at 40Gb/s/channel; Section 4 outlines the design and synthesis of band-pass OFs using optical resonators. Optical band-pass Butterworth/Chebyshev filters are obtained for optical communication windows; Section 5 gives comparisons and conclusions of the filter pass-band effects on 40Gb/s optical signals under various modulation formats such as CS-RZ format, VSB etc.; In Section 6 the detailed design of optical HBFs is described. In particularly, the third and fifth order of FIR HBFs and IIR HBFs are investigated; Section 7 gives conclusions and recommends future works.

2 Generic issues of OFs

2.1 Photonic transfer function, SFG and realisation

Digital filters are characterized by their transfer functions. In general, the transfer function of discrete filters can be expressed as [**19**]:

$$H(z)=\frac{b_0+b_1z^{-1}+b_2z^{-2}+.....+b_Mz^{-M}}{1+a_0+a_1z^{-1}+a_2z^{-2}+.....+a_Nz^{-N}}$$

Eq. 1

The discrete system is (i) Stable if and only if all poles lie in the open unit-disk of complex plane (not including the boundary); (ii) Marginally stable if and only if all poles lie in the unit-disk and non-repeated poles can be located on the unit circle; (iii) Unstable if and only if one or more poles located outside the closed unit-disk or having one or more repeated poles located on unit

circle. Thus stability of the system depends on the pole location. If the transfer function of a filter could be represented as a polynomial (all $a_{i=0}$) that filter is called FIR (finite-duration unit-impulse response) filter. Because of that characteristic, FIR filters whose all poles are located at the origin are also called all-zero filter. Otherwise they are IIR filters in general. Therefore, IIR filters are more general than the others because they include the conventional FIR filters with exactly linear phase and all-pass filters [**20**].

In the analysis and synthesis of OFs, we employ a graphical method to yield the transfer function so that a quick inspection of their characteristics of any photonic circuits can be revealed. SFG technique for representing a set of linear algebraic equations and represented by a network of transmittances of direct branches which connect at nodes and is simply a pictorial representation of the simultaneous algebraic equations describing a system a graphically displays the flow of signals through a system. The SFG method can be interpreted as a transformation of either the method of successive substitutions of simultaneous equations or the transfer matrix method to a topological approach. This method has been widely used with great success in the diverse fields of electronics, digital signal processing and control systems since its development by Manson in the 1950s [**21**], [**22**], [**23**]. Thus it can be applied to any linear time-invariant systems [**21**].

The optical transfer gain of the optical network or circuit can be obtained from the SFG and application of the optical Mason's rule makes the process quantitative by permitting us to compute easily the actual transmission gain, T, between any input X_i, and any output X_o. The rule states that [**16**]:

$$T = \frac{\sum P_k \Delta_k}{\Delta} \qquad \text{Eq. 2}$$

where the subscript k refers to the k^{th} different direct path from the input X_i, to the output X_o and the corresponding path gain is P_k. The realisation of OFs, in general, can follow two structures that can yield the same filtering effects, the cascade type and parallel configurations.

2.1.1 Cascade realization

Let z_k and p_k are the zeros and poles of the transfer function, the quadratic terms of only real coefficients can be obtained by combining each pair of complex poles or zeros together as follows.

$$\begin{aligned}\left(1-z_k z^{-1}\right)\left(1-z_k{}^{*} z^{-1}\right)&=\left(1+\alpha_{1k} z^{-1}+\alpha_{2k} z^{-2}\right)\\ \left(1-p_k z^{-1}\right)\left(1-p_k{}^{*} z^{-1}\right)&=\left(1+\beta_{1k} z^{-1}+\beta_{2k} z^{-2}\right)\end{aligned}$$

Eq. 3

Let $z_k = A + jB$, then $z_k^{*} = A - jB$. Thus

$$\begin{aligned}&\left(1-z_k z^{-1}\right)\left(1-z_k{}^{*} z^{-1}\right)=\left[1-(A+jB)z^{-1}\right]\left[1-(A-jB)z^{-1}\right]\\ &=1-2Az^{-1}+\left(A^2+B^2\right)z^{-2}\end{aligned}$$

Eq. 4

Similarly for p_k, the quadratic terms which contain only real numbers are computed and allowed to express in a more easily form.

In fact, the overall system transfer function equation can be expressed in general as follows.

$$H_{BPF}\left(z^{-1}\right)=\prod_{k=1}^{N}\frac{\left(1+\alpha_{1k} z^{-1}+a_{2k} z^{-2}\right)}{\left(1+\beta_{1k} z^{-1}+\beta_{2k} z^{2}\right)}$$

Eq. 5

Parallel realization

In the case of complex poles, their corresponding residues are also complex. However they are conjugated in pair so that they can yield quadratic factors. And so are the real poles. By combining them all together, the transfer function of any filters can be expressed in parallel type as follows.

$$H_{BPF}\left(z^{-1}\right)=\sum_{k=0}^{M-N}G_k z^{-k}+\sum_{k=1}^{N_r}\frac{A_k}{1-p_k z^{-1}}+\sum_{k=1}^{N}\frac{B_k\left(1-z_k z^{-1}\right)}{\left(1-r_k z^{-1}\right)\left(1-r_k{}^{*} z^{-1}\right)}$$

Eq. 6

2.2 Optical Resonance circuit

The characteristics of optical resonators had been studied and the design in all-pole, all-zero optical circuits, and single-pole single-zero resonator (APOC, AZOC, and SPSZR) are provided. These are applications took from optical couplers, in particular, the 4-port (or 2x2) optical couplers and 6-port (3x3) optical couplers.

2.2.1 The Double-coupler Optical Resonators

There are two kinds of double-coupler resonator. One is the double-couple feed-forward optical resonator (DCFFOR) and the other is the double-couple feed-back optical resonator (DCFBOR). DCFFOR provides 100% of light power will go straight forward from one to another coupler, while DCFBOR could take some percentages of light power back after travelled straight forward like DCFFOR.

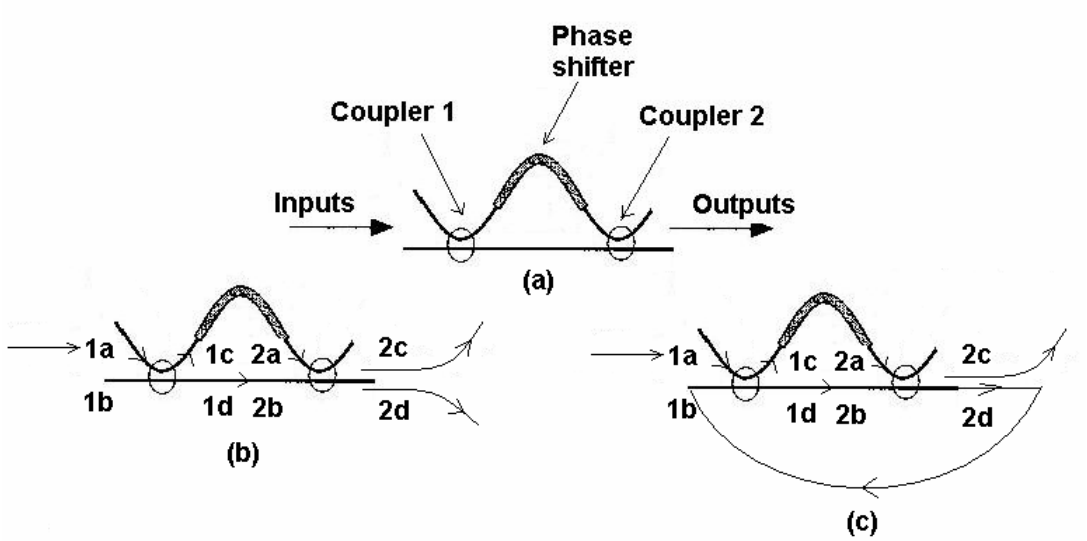

Figure 1*: Schematic diagram of fiber coupler (a) in general form (b) DCFFOR (c) DCFBOR.*

In order to study the characteristics of these two kinds of double-coupler optical resonators, the SFG is represented to yield transfer functions graphically.

2.2.1.1 The circuit configuration and characteristics of a Double-coupler Feed-Forward Optical Resonator (DCFFOR)

Figure 2 shows the circuit configuration of a DCFFOR which can be can be redrawn as

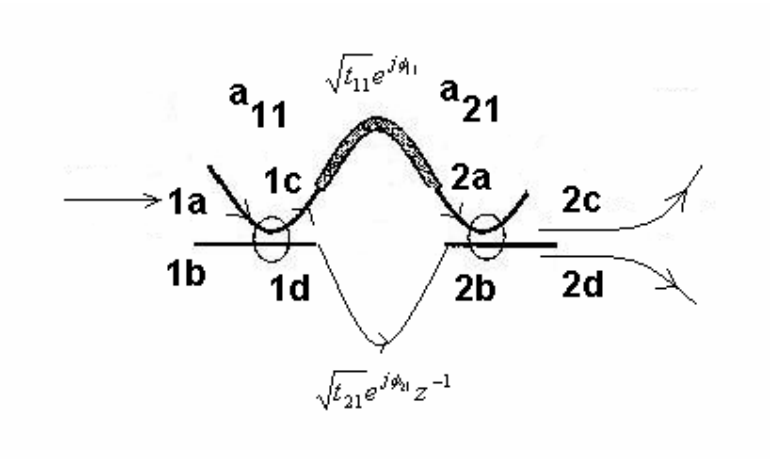

Figure 2: The circuit configuration of a DCFFOR.

This circuit configuration of a DCFFOR in the above figure is characterized under these following notations where input and output ports are (1a, 1b) and (2c, 2d) respectively. The optical transmittance coefficients are defined as: a_{pq}: intensity coupling coefficient of p^{th} coupler and q^{th} subsystem; t_{pq}: intensity transmission coefficient of p^{th} coupler and q^{th} subsystem; ϕ_{pq}: optical phase shift of p^{th} fiber path and q^{th} subsystem.. As $t_{pq} \geq 1$, an optical gain G is required by adding an erbium-doped fiber amplifier (EDFA) into the fiber path. In fact, by changing G and phase shift, different resonators can be designed for a 4-port directional coupler, 2 × 2 directional coupler. In general case, let the percentage to be denoted as γ, the intensity coupling loss, so that the light power remains in the other port will be (1- γ). In complex number, $j = \sqrt{-1}$, so –j will represent a -90^0 phase shift for cross coupler waveguides.

Let the amplitudes at the input and output ports are (E_{1a}, E_{1b}) and (E_{2c}, E_{2d}) respectively, at the feedback path:

$$E_{1b} = \sqrt{t_{21}}e^{j\phi_{21}}z^{-1} \qquad \text{(assuming the path length difference is } \Delta L) \qquad \textbf{Eq. 7}$$

where $\sqrt{t_{21}} = \sqrt{G}e^{-\alpha L}$ and α is the amplitude attenuation coefficient. **Eq. 8**

The graphical method can be applied to obtain the transfer function between two nodes. That type of method named as SFG technique for representing a set of linear algebraic equations by a

'graph'. Assuming that the light power gets through both input ports (1a, 1b), and the SFG is shown in Figure 3

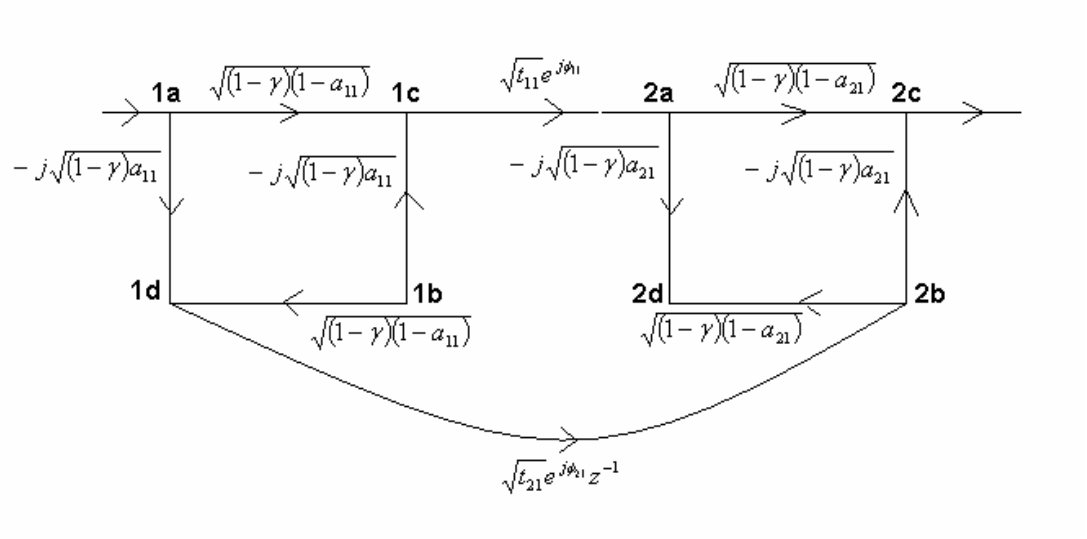

Figure 3*: The corresponding SFG of* Figure 2.

By applying Mason's rule, the transfer function that is taken from the output port 2c and 2d to the input port 1a is obtained as

$$
\begin{aligned}
H_{FF} &= \frac{E_{2c}}{E_{1a}} + \frac{E_{2d}}{E_{1a}} \\
&= \left(-j\sqrt{a_{21}(1-a_{11})} + \sqrt{(1-a_{11})(1-a_{21})}\right)(1-\gamma)\sqrt{t_{11}}e^{j\phi_{21}} - \left(j\sqrt{(1-a_{21})} + \sqrt{a_{21}}\right)(1-\gamma)\sqrt{t_{21}a_{11}}e^{j\phi_{21}}z^{-2} \\
&= \left[\sqrt{(1-a_{21})} - j\sqrt{a_{21}}\right](1-\gamma)\sqrt{t_{11}(1-a_{11})}e^{j\phi_{11}} - \left[j\sqrt{(1-a_{21})} + \sqrt{a_{21}}\right](1-\gamma)\sqrt{t_{21}a_{11}}e^{j\phi_{21}}z^{-2}
\end{aligned}
$$

Eq. 9

This shows that the poles of this filter are located at the origin. Therefore, the transfer function of a DCFFOR is an all-zero system.

i. The circuit configuration and characteristics of a Double-coupler Feed-Back Optical Resonator (DCFBOR): Figure 4 shows the circuit configuration of a DCFFOR.

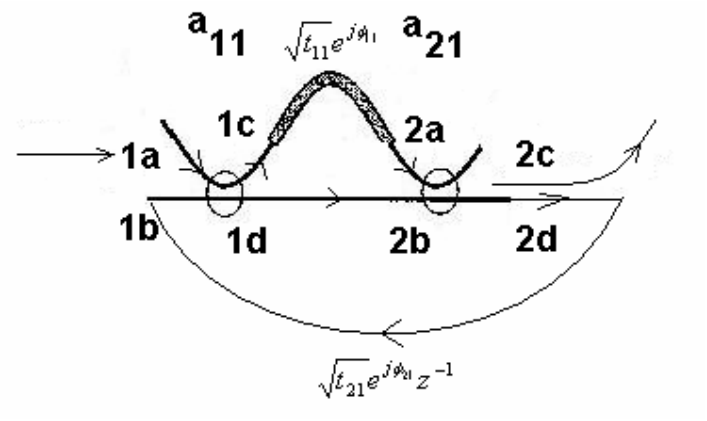

Figure 4*: The circuit configuration of a DCFFOR.*

The corresponding SFG of the DCFFOR is shown in Figure 4.

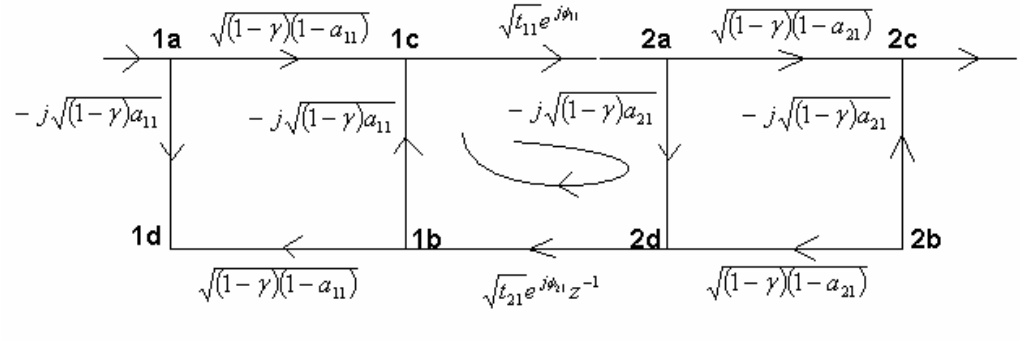

Figure 5: The corresponding SFG of the circuit in Figure 4.

Applying the Manson's gain rule (eq.2) yields the transfer function from input port 1a to output port 2c as

$$\frac{E_{2c}}{E_{1a}} = \frac{(1-\gamma)e^{j\phi_{11}}\sqrt{t_{11}(1-a_{11})(1-a_{21})}}{1+(1-\gamma)\sqrt{t_{11}t_{21}a_{11}a_{21}}e^{j(\phi_{11}+\phi_{21})}z^{-2}} \qquad \text{eq. 10}$$

Because after the cancellation of the common factors in the denominator and numerator, Eq. 3 still yields $b_i = 0$, this filter is an all-pole system, that is all zeros are located at the origin.

2.2.2 A 6-port optical resonator

A ring resonator with threshold symmetry was proposed as a planar realization of the symmetric 3 × 3 fiber coupler to be used in compact integrated optics interferometers and passive optical signal processing schemes [**28**]. The specific single-pole and single-zero system [**10**] is

constructed by using a 3 × 3 optical direction coupler with two optical feed-back paths which is drawn in figure 3.6. This 3 × 3 optical directional coupler is consisted of two 2 × 2 directional couplers that sharing the common optical interconnection area. The use of two 2 × 2 directional couplers allows access to the light within the ring and in some ways; it provides the symmetric feature for this 3 × 3 optical directional coupler. The advantage is that we can fully control the optical phase shift or phase delay between the neighbouring of these two 2 × 2 optical directional couplers.

2.2.2.1 A 3 × 3 coupler optical resonator

The circuit configuration of a 3 × 3 optical directional coupler is shown in Figure 6 below. There are two feed-back paths which are shown by using directional arrows in order to indicate the direction of the couplers and the common section is in the middle.

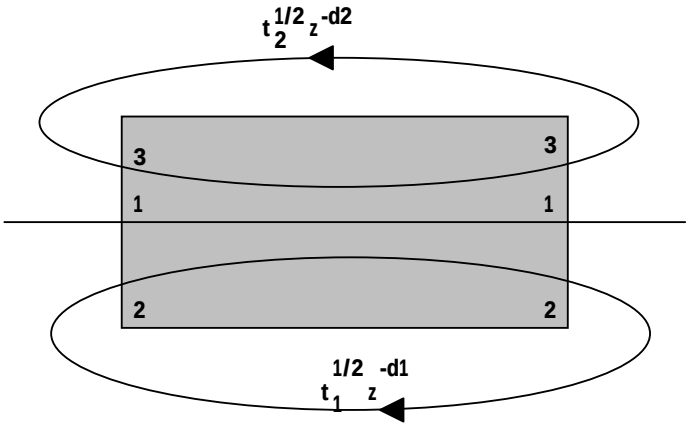

Figure 6: The circuit configuration of a 3 × 3 optical directional coupler.

The order of delay is set as 1, for a general case. All notations had stated in this 3 × 3 optical directional coupler having the same meaning as that of the optical double-coupler. So, there are two feed-back paths across the upper and lower coupler-parts as above.

2.2.2.2 The characteristics of a 3 × 3 coupler Optical Resonator

Similar to the analyses of DCFFOC and DCFBOC, the SFG method (as shown in Figure 7) and the Manson's rule are applied to yield the transfer function between the input and output ports (1d, 1a).

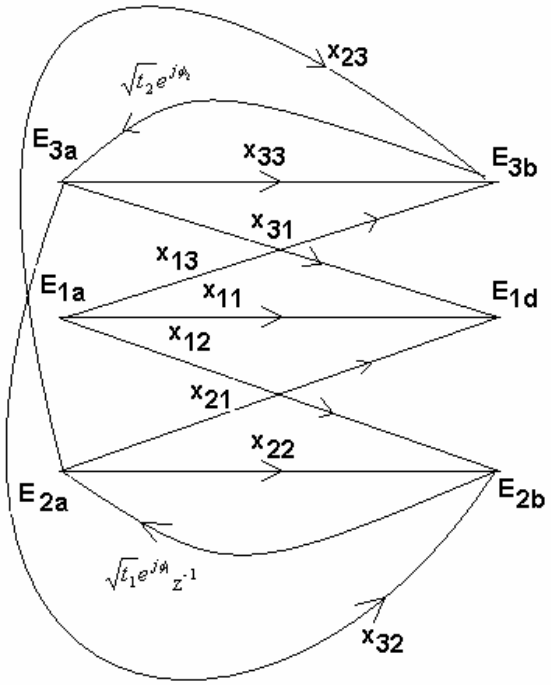

Figure 7: The corresponding SFG of the circuit of Figure 6.

Hence, the transfer function can be obtained as

$$\frac{E_{1d}}{E_{1a}} = \frac{-2\left(\sqrt{t_{1k}}e^{j\phi_{1k}}z^{-1} - \sqrt{t_{1k}t_{2k}}e^{j(\phi_{1k}+\phi_{2k})}z^{-1} + \sqrt{t_{2k}}e^{j\phi_{2k}}\right)}{\left(2-\sqrt{t_{1k}}e^{j\phi_{1k}}z^{-1}\right)\left(2-\sqrt{t_{2k}}e^{j\phi_{2k}}\right)}$$

Eq. 11

Because after the cancellation of the common factors in the denominator and numerator, Eq. 3 is still achieved $a_i \neq 0$ and $b_i \neq 0$ and only one root is removed from each denominator and numerator; it is observed as a case for designing a pole and a zero system. *Figure 25* used the terminology "Single-pole Single-zero Resonator (SPSZR)" to name this kind of optical resonator.

2.3 Realization Methods

The realization method is a technique that allows designers some options in order to implement the real optical filers in practice. There are two structures that available to perform the same filtering functions. They are the cascaded types and parallel type [**27**]. The cascaded type allows

expressing the system function as a multiplication form while parallel type provides the same function characteristics but in the sum of basic elements.

In order to consider the whole process generally, the block diagram will be drawn. In the case of cascaded type, the block diagram is called tandem and that of parallel type is named as parallel block diagram. The SPSZRs, APOCRs, and AZOCRs are considered inside the performance of optical directional couplers in particular and optical resonators, interferometers, optical delay line circuits in general. By using these three different types of resonators, the cascaded and parallel form realization could be formed. A combination of SPSZRs and APOCRs is denoted as Type 1 and that of the APOCRs and AZOCRs as Type 2.

2.3.1 The Cascaded Realization Method

Cascaded Realization is to perform the transfer function as a multiplication of all basic elements by combining each pair of complex conjugated poles or zeros into quadratic terms. This quadratic form will be real coefficients so that the transfer function will be expressed in a clear form without the imaginary parts.

2.3.1.1 The cascading realization type 1

Type 1 is about combining SPSZRs and APOCRs together. Both of these resonators had been studied in the Optical Components for Designing Optical Band-pass Filters.

- SPSZR: Leaning on the transfer function between the output and input port of a planar 3 × 3 directional optical coupler, if (p, z) is a pair of pole-zero which is also the roots of the numerator and denominator of the transfer function, then

$$p = \frac{1}{2}\sqrt{t_{1k}}e^{j\phi_{1k}} \rightarrow t_{1k} = \left(\frac{2p}{e^{j\phi_{1k}}}\right)^2$$

Eq. 12

$$-\frac{2pz^{-1}}{1-2pz^{-1}} = \sqrt{t_{2k}}e^{j\phi_{2k}} = Q \rightarrow t_{2k} = \left(\frac{Q}{e^{j\phi_{2k}}}\right)^2$$

Eq. 13

Thus, by choosing the appropriate optical phase shifts ϕ, the intensity transmission coefficients t will be computed by using the above relation equations.

- APOCRs: Refer to the transfer function between the output port and input port of the 4-port (2 × 2) directional coupler, the location of a pole in the case of the zero is at origin is

$$p = -(1-\gamma)\sqrt{a_{11}a_{21}t_{11}t_{21}}\,e^{j(\phi_{11}+\phi_{21})}$$

Eq. 14

thus

$$\rightarrow \sqrt{a_{11}a_{21}t_{11}t_{21}} = -\frac{p_1}{(1-\gamma)e^{j(\phi_{11}+\phi_{21})}} = X$$
$$\rightarrow t_{11}t_{21} = \frac{X^2}{a_{11}a_{21}}$$

Eq. 15

By choosing the intensity coupling loss γ, assuming the appropriate optical phase shift ϕ, intensity coupling coefficients a, the intensity transmission coefficients t can be obtained.

2.3.1.2 The cascading realization type 2

Unlikely, the Cascading Realization Type 2 is about combination of APOCRs and AZOCRs (while in type 1, the combination of all SPSZRs had been concerned). Thus, the overall system transfer function equation will be expressed as the form where the multiplication between APOCR and AZOCR is considered as follow.

$$H_{BPF}\left(z^{-1}\right) = \prod H_{APOCRi}\left(z^{-1}\right)\cdot H_{AZOCRi}\left(z^{-1}\right)$$

Eq. 16

So, each pole or zero will form its own APOCR or AZOCR respectively. For instance, designing the 8th order of Butterworth Band pass OF, there is the case where 8 APOCRs and 8 AZOCRs combined.

Since the general transfer function stated above is in the first order of z^{-1}, that means the delay coefficient or the path length difference is set at 1. So, if the system appears the poles and zeros in either pure real or pure imaginary or conjugated pairs, that delay can be expressed as more delay, say the second order or more.

- APOCRs: same as above.
- AZOCRs: similar to APOCR, refer to the transfer function between output port and input port of the 4-port (2 × 2) directional coupler, the location of a zero in the case of the pole is at origin is

$$z = \sqrt{\frac{a_{11}a_{21}t_{21}}{(1-a_{11})(1-a_{21})t_{11}}}e^{j(\phi_{21}-\phi_{11})}$$

Eq. 17

By choosing the phase shifts ϕ such that

$$z = Me^{j(\phi_{21}-\phi_{11})}$$

Eq. 18

where $$M = \sqrt{\frac{a_{11}a_{21}t_{21}}{(1-a_{11})(1-a_{21})t_{11}}}$$

Eq. 19

Assume a value for intensity coupling coefficients a, the intensity transmission coefficients t can be obtained as

$$\frac{t_{21}}{t_{11}} = \frac{M^2}{N}$$

Eq. 20

Where $$N = \frac{a_{11}a_{21}}{(1-a_{11})(1-a_{21})}$$

2.3.2 The Parallel Realization Methods

Parallel Realization is to represent the transfer function in the parallel form so that it is the sum of all basic elements (just like working in electronics' point of view). The idea is that complex conjugated poles and complex conjugated residues can make quadratic real coefficients. These real coefficients will form a clear formula to rewrite the old transfer function.

2.3.2.1 The parallel realization type 1

After rewrite the transfer function into the Parallel Realization form, stated in the Literature Reviews, depending on how many basic elements appear in that transfer function, the number of subsystems is counted. Note that basic element could be just a gain itself.

The same process as Cascading Realization Type 1 is carried on by using SPSZRs and APOCRs.

2.3.2.2 The parallel realization type 2

Working on Parallel Realization is working on the Parallel Realization form, not the old transfer function, so that the zeroes' locations might slightly different from the old one.

After recognizing the new pole-zero, the same process that had been carried in the Cascading Realization Type 2 is required.

2.4 Optical FIR HBFs

Optical FIR HBFs are designed by feed-forward waveguides and their impulse responses are limited in finite time. One of the attractive properties of FIR filters is that they can reach the exact linear phase where that of IIR filters could not be possible to achieve. In the next two sections the design techniques of the optical FIR HBFs when the number of interferometers is set at two and three are considered.

Because these optical FIR HBFs are composed of optical waveguides operating such as optical phase shifts, 2×2 directional couplers (4-port directional couplers), the design method is that by varying these optical phase shifts, intensity coupling coefficients, intensity transmission

coefficients so that the systems stay in the stable conditions. There is noted that the coupling loss is set to be at 0% that means under the ideal condition through out this chapter.

2.4.1 The Design Techniques of the Optical FIR HBFs

Figure 6.1 below shows the two kinds of novel 2 × 2 circuit configurations for FIR HBFs which is extracted from figure 2 in the paper of Jungji [14].

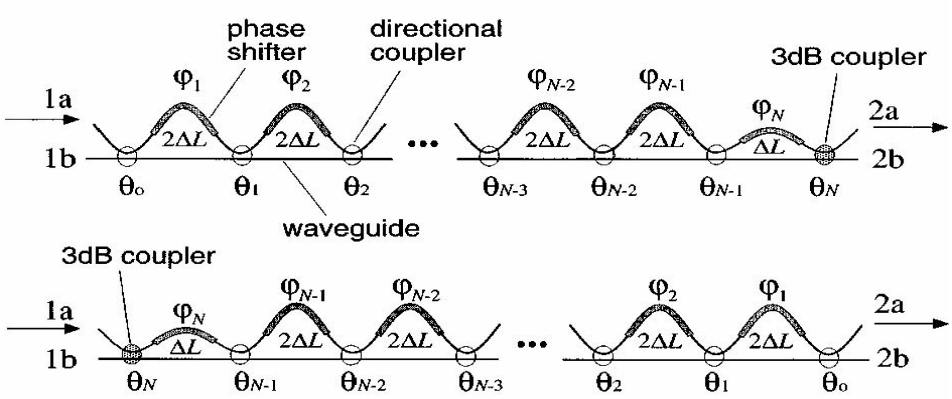

Figure 8: Two kinds of novel 2 × 2 circuit configurations for FIR HBFs.

This is clear that they are can be transformed into each other with a symmetric transformation which reverses their input and output ports and still satisfied the power half-band property. They are composed by (N-1) MZI's with a path length difference of 2ΔL and one MZI with a single path length difference of ΔL. If the input light-wave port is assumed to be 1a, the transfer function of the bar function is taking from the input light-wave port 1a to the output port 2a. And transfer function of the cross function is taking form that input port to other output port which is 2b.

FIR HBFs exhibit the minimum number of couplers is considered as two that corresponds to the order of that three. The order of the system is the delay which corresponds to the difference path length in the system. Because there will always be a MZI's with a single path length difference at the end and a number of MZI's with double path length difference, FIR HBFs will always be designed in odd order. The characteristics and the design techniques of optical FIR HBFs are

discussed for two particular cases when the numbers of interferometers are two and three in the followings.

2.4.2 The Characteristics and Transfer functions of the Optical FIR HBFs length-2

This is the simplest case to design an optical FIR HBF. It is composed by a single path length difference together with a double path length difference in order to compute the optical FIR HBF. The circuit configurations and transfer functions of its bar and cross functions are described below.

2.4.2.1 The Transfer functions of the optical FIR HBF length-2

The transfer functions of the optical FIR HBF depend on that of the cross and the bar functions in which two output port are received. The cross function in this case is the transfer function taking place from input port 1a to output port 3d and bar function is taking from input port 1a to output port 3c. Note that this is assumed that only one input port 1a that carries light-wave into the system. Because the optical FIR HBF has no feed-back loop existed in the system, Manson's rule stated the transfer function should be the summation of all of the path gains which means that there is no denominator.

- *The transfer function of the cross function*

There are three path ways to let the light-wave from input port 1a to output port 3d which correspond to three path gains P_1, P_2 and P_3 respectively.

$$\begin{aligned} P_1 &= (1a)(1c)(2a)(2c)(3a)(3d) \\ &= \left[\sqrt{(1-\gamma)(1-a_{11})}\right]\left[\sqrt{t_{21}}e^{j\phi_{21}}z^{-2}\right]\left[\sqrt{(1-\gamma)(1-a_{21})}\right]\left[\sqrt{t_{12}}e^{j\phi_{12}}z^{-1}\right]\left[-j\sqrt{(1-\gamma)a_{12}}\right] \\ &= -j(1-\gamma)\sqrt{(1-\gamma)(1-a_{11})(1-a_{21})a_{12}t_{21}t_{12}}e^{j(\phi_{21}+\phi_{12})}z^{-3} \end{aligned} \qquad \text{Eq. 22}$$

$$\begin{aligned} P_2 &= (1a)(1d)(2b)(2c)(3a)(3d) \\ &= \left[-j\sqrt{(1-\gamma)a_{11}}\right]\left[\sqrt{t_{11}}e^{j\phi_{11}}\right]\left[-j\sqrt{(1-\gamma)a_{21}}\right]\left[\sqrt{t_{12}}e^{j\phi_{12}}z^{-1}\right]\left[-j\sqrt{(1-\gamma)a_{12}}\right] \\ &= j(1-\gamma)\sqrt{(1-\gamma)a_{11}a_{21}a_{12}t_{11}t_{12}}e^{j(\phi_{11}+\phi_{12})}z^{-1} \end{aligned} \qquad \text{Eq. 23}$$

$$
\begin{aligned}
P_3 &= (1a)(1c)(2a)(2d)(3b)(3d) \\
&= \left[\sqrt{(1-\gamma)(1-a_{11})}\right]\left[\sqrt{t_{21}}e^{j\phi_{21}}z^{-2}\right]\left[-j\sqrt{(1-\gamma)a_{21}}\right]\left[\sqrt{t_{21}}e^{j\phi_{21}}\right]\left[\sqrt{(1-\gamma)(1-a_{12})}\right] \\
&= -j(1-\gamma)\sqrt{(1-\gamma)(1-a_{11})(1-a_{12})a_{21}t_{21}}e^{j2\phi_{21}}z^{-2}
\end{aligned}
\qquad \text{Eq. 24}
$$

Thus, using Mason'gain rule the transfer function of a cross function is the summation of P_1 through P_3 since there is no loop existing in this case.

$$
\begin{aligned}
P_{cross1} &= j(1-\gamma)\sqrt{(1-\gamma)a_{11}a_{21}a_{12}t_{11}t_{12}}e^{j(\phi_{11}+\phi_{12})}z^{-1} \\
&- j(1-\gamma)\sqrt{(1-\gamma)(1-a_{11})(1-a_{12})a_{21}}t_{21}e^{j2\phi_{21}}z^{-2} - j(1-\gamma)\sqrt{(1-\gamma)(1-a_{11})(1-a_{21})a_{12}t_{21}t_{12}}e^{j(\phi_{21}+\phi_{12})}z^{-3}
\end{aligned}
\qquad \text{Eq. 25}
$$

- *The transfer function of the bar function*

There are also three path ways to let the light-wave from input port 1a to output port 3c which correspond to three path gains P_1, P_2 and P_3 respectively. Similarly, the bar function can be derived.

$$
\begin{aligned}
P_1 &= (1a)(1c)(2a)(2c)(3a)(3c) \\
&= \left[\sqrt{(1-\gamma)(1-a_{11})}\right]\left[\sqrt{t_{21}}e^{j\phi_{21}}z^{-2}\right]\left[\sqrt{(1-\gamma)(1-a_{21})}\right]\left[\sqrt{t_{12}}e^{j\phi_{12}}z^{-1}\right]\left[\sqrt{(1-\gamma)(1-a_{12})}\right] \\
&= (1-\gamma)\sqrt{(1-\gamma)(1-a_{11})(1-a_{21})(1-a_{12})t_{21}t_{12}}e^{j(\phi_{21}+\phi_{12})}z^{-3}
\end{aligned}
$$

$$
\begin{aligned}
P_2 &= (1a)(1d)(2b)(2c)(3a)(3c) \\
&= \left[-j\sqrt{(1-\gamma)a_{11}}\right]\left[\sqrt{t_{11}}e^{j\phi_{11}}\right]\left[-j\sqrt{(1-\gamma)a_{21}}\right]\left[\sqrt{t_{12}}e^{j\phi_{12}}z^{-1}\right]\left[\sqrt{(1-\gamma)(1-a_{12})}\right] \\
&= -(1-\gamma)\sqrt{(1-\gamma)(1-a_{12})a_{11}a_{21}t_{11}t_{12}}e^{j(\phi_{11}+\phi_{12})}z^{-1}
\end{aligned}
\qquad \text{Eq. 26}
$$

$$
\begin{aligned}
P_3 &= (1a)(1c)(2a)(2d)(3b)(3c) \\
&= \left[\sqrt{(1-\gamma)(1-a_{11})}\right]\left[\sqrt{t_{21}}e^{j\phi_{21}}z^{-2}\right]\left[-j\sqrt{(1-\gamma)a_{21}}\right]\left[\sqrt{t_{21}}e^{j\phi_{21}}\right]\left[-j\sqrt{(1-\gamma)a_{12}}\right] \\
&= -(1-\gamma)\sqrt{(1-\gamma)(1-a_{11})a_{21}a_{12}}t_{21}e^{j2\phi_{21}}z^{-2}
\end{aligned}
$$

Hence, substituting into (2), the transfer function of a cross function is the summation of P_1 through P_3 since there is no loop existing in this case.

$$
\begin{aligned}
P_{bar1} &= -(1-\gamma)\sqrt{(1-\gamma)(1-a_{12})a_{11}a_{21}t_{11}t_{12}}e^{j(\phi_{11}+\phi_{12})}z^{-1} \\
&-(1-\gamma)\sqrt{(1-\gamma)(1-a_{11})a_{21}a_{12}}t_{21}e^{j2\phi_{21}}z^{-2} + (1-\gamma)\sqrt{(1-\gamma)(1-a_{11})(1-a_{21})(1-a_{12})t_{21}t_{12}}e^{j(\phi_{21}+\phi_{12})}z^{-3}
\end{aligned}
\qquad \text{Eq. 27}
$$

2.4.2.2 The Circuit configurations of the optical FIR HBF length-2

Figure 9 below shows the circuit configuration of the optical FIR HBF when the number of interferometers is two. It is composed of a MZI's with a path length difference of 2ΔL and another MZI's with a single path length difference of ΔL.

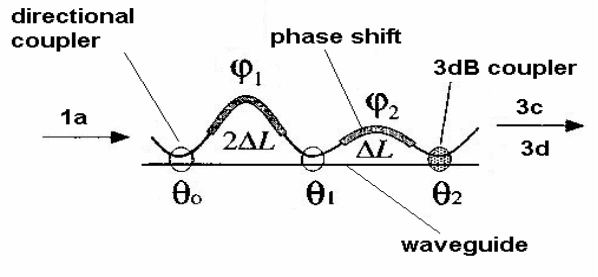

Figure 9: FIR HBFlength-2.

Figure 10 is the corresponding SFG that has been drawn from *Figure 9* above.

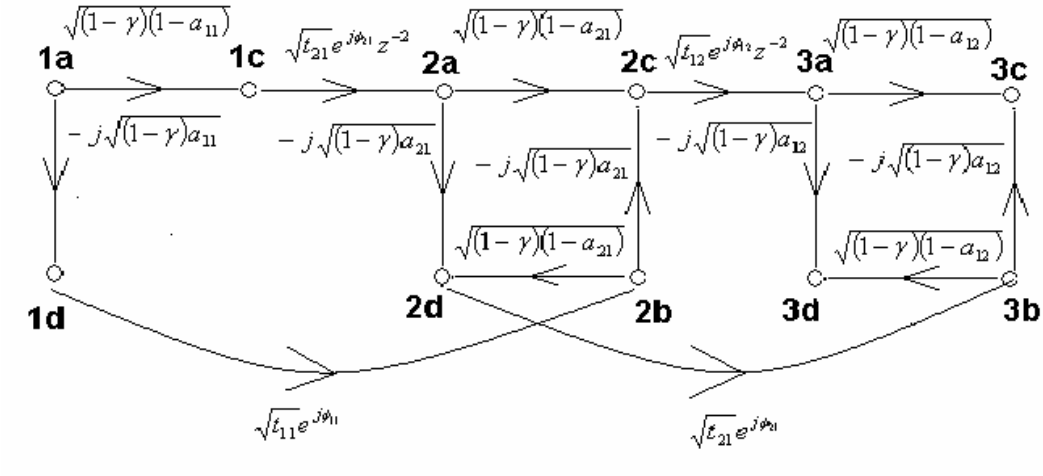

Figure 10: Corresponding SFG representation of Figure 9.

From the above SFG representation, the transfer functions of the bar and cross functions can be obtained without difficulty.

i. Simulation results

In the case of two interferometers (i.e. N = 2), there are 2 zeros and 2 poles (at the origin) in the system. For ideal condition, as mentioned in the introduction all calculations had been done in the case of no loss (i.e. $\gamma = 0\%$). In order to satisfy the stability of the system, the chosen values for optical phase shifts, intensity transmission coefficients as well as intensity coupling coefficients are set. The *Table 1* and *Table 2* show the chosen values of the bar and the cross transfer function respectively.

Intensity coupling coefficients (a_{pq})		
a_{11}	a_{12}	a_{21}
0.9	0.2	0.3
Intensity transmission coefficients (t_{pq})		
t_{11}	t_{12}	t_{21}
1	2	3
Optical phase shift (Φ_{pq})		
ϕ_{11}	ϕ_{12}	ϕ_{21}
Π	$\pi/2$	$\pi/3$

Table 1: Optical FIR HBF when N = 2: The chosen parameters of the transfer function of the bar function.

Intensity coupling coefficients (a_{pq})		
a_{11}	a_{12}	a_{21}
0.3	0.5	0.3
Intensity transmission coefficients (t_{pq})		
t_{11}	t_{12}	t_{21}
8	2.7	1.1
Optical phase shift (Φ_{pq})		
ϕ_{11}	ϕ_{12}	ϕ_{21}
$-\pi$	$-\pi/2$	$-\pi/3$

Table 2: Optical FIR HBF when N = 2: The chosen parameters of the transfer function of the cross function.

The magnitude responses and phase responses of the transfer functions of the bar and the cross functions are shows in Figure 11 and *Figure 12* respectively.

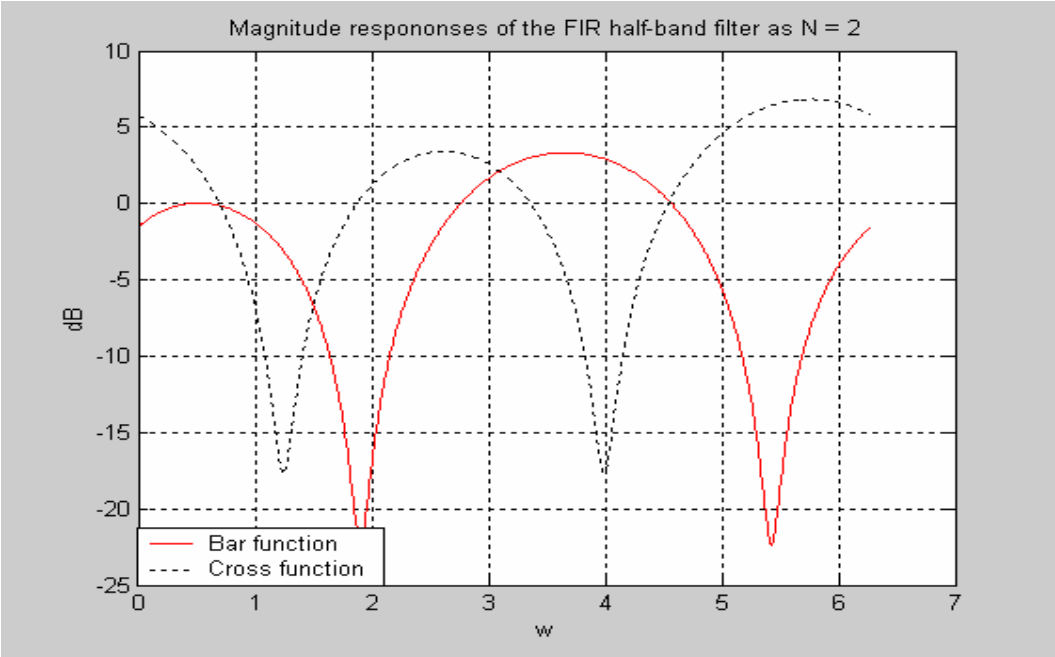

Figure 11: The optical FIR HBF length-2: the magnitude responses.

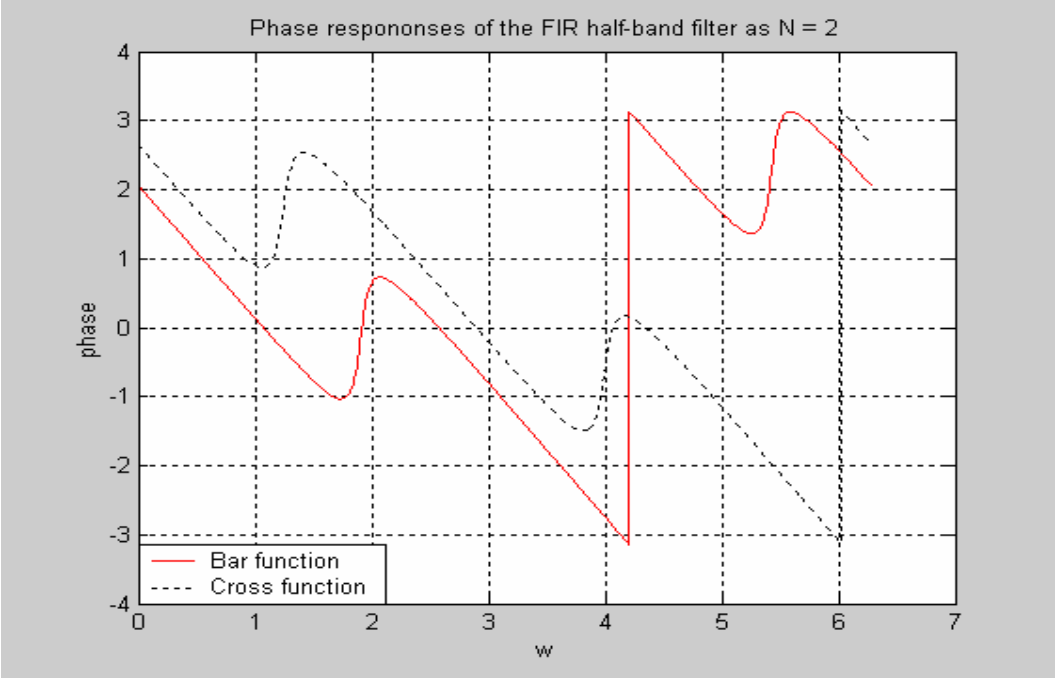

Figure 12: The optical FIR HBF length-2: the phase responses.

Because the transfer functions of the bar and the cross functions are the ratios between the input port 1a and the output 3c, 3d respectively; the light-wave powers need to satisfy the reserved energy property. This shows in their magnitude responses where there is the energy of the bar

function pulls up, that of the cross function pulls down. Although their phase responses did not achieve the exact linear phase, they still show the linear phase in such long periods.

In this case when the optical FIR HBF is considered when the number of interferometers is two, the frequency responses with respected to the transfer function of the cross and the bar functions are having the same property. Thus, after the transmission the light-wave from either output 3c or 3d can be taken out.

The Characteristics and Transfer functions of the Optical FIR HBFs length-3

As the number of interferometers increases, that means the order of the optical FIR HBF also increases. This occurs due to the number of the path length differences which increase the delays into the system. Similarly to the previous Sub-section, the transfer functions of the bar and the cross functions will be derived, the circuit configuration and corresponding SFG representation are illustrated in *Figure 13* and *Figure 14* in the next Sub-section.

i. The Circuit configurations of the optical FIR HBF length-3

Indeed, the circuit configuration of the optical FIR HBF when number of interferometers is three is composed of two MZI's with a path length difference of 2ΔL and another MZI's with a single path length difference of ΔL as illustrated in the *Figure 13* below.

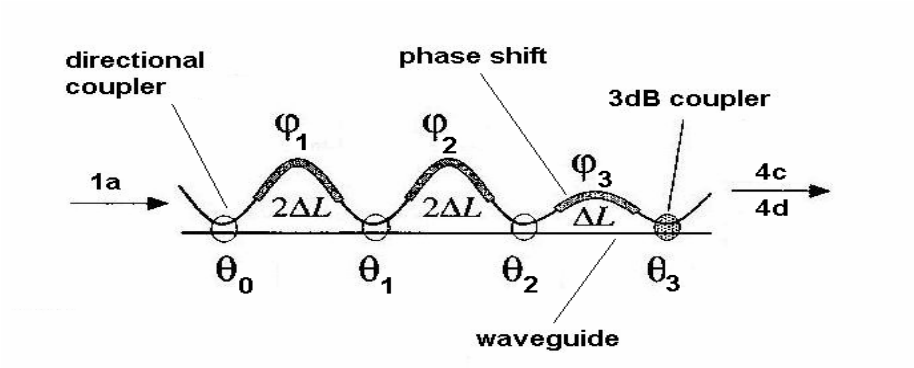

Figure 13: Circuit configuration of the optical FIR HBFs when the number of interferometers is 3.

And the corresponding SFG representation of figure 6.7 is illustrated in the following *Figure 14*.

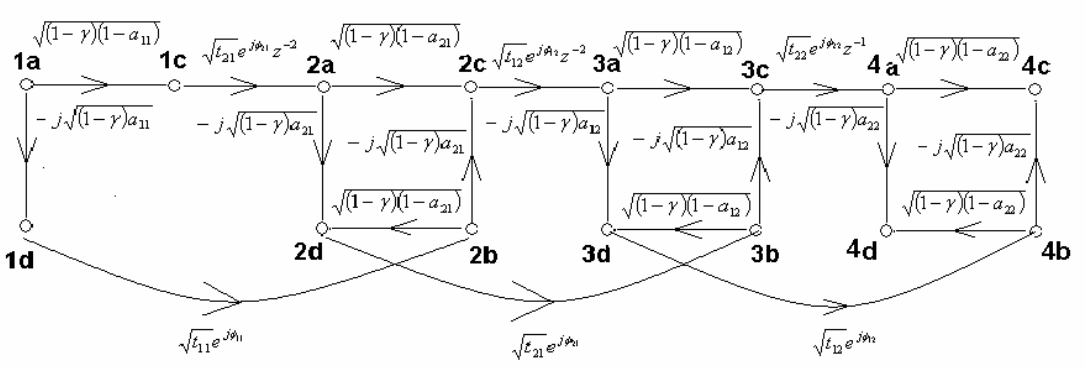

Figure 14: The SFG Representation of the optical FIR HBFs when the number of interferometers is 3.

The transfer function of the bar function is the intensity power that takes between the input power of node 1a and output power of node 4c. And that of the cross function is the ratio between input light-wave 1a and output port 4d.

2.4.2.3 The Transfer functions of the optical FIR HBF length-3

Again because of no feed-back loops, Manson's gain rule [Eq. 2] stated that transfer function depended only on the paths gains.

- *Transfer function of the bar function*

Transfer function of bar function (from 1a to 4c) is derived as follows. There are 5 path ways go from 1a through 4c which correspond to the following path gains.

$$\begin{aligned} P_1 &= (1a)(1c)(2a)(2c)(3a)(3c)(4a)(4c) \\ &= \left[\sqrt{(1-\gamma)(1-a_{11})}\right]\left[\sqrt{t_{21}}e^{j\phi_{21}}z^{-2}\right]\left[\sqrt{(1-\gamma)(1-a_{21})}\right]\left[\sqrt{t_{12}}e^{j\phi_{12}}z^{-2}\right] \\ &\left[\sqrt{(1-\gamma)(1-a_{12})}\right]\left[\sqrt{t_{22}}e^{j\phi_{22}}z^{-1}\right]\left[\sqrt{(1-\gamma)(1-a_{22})}\right] \\ &= (1-\gamma)^2\sqrt{(1-a_{11})(1-a_{21})(1-a_{12})(1-a_{22})t_{21}t_{12}r_{22}}\,e^{j(\phi_{21}+\phi_{12}+\phi_{22})}z^{-5} \end{aligned} \quad \text{Eq. 28}$$

$$
\begin{aligned}
P_2 &= (1a)(1d)(2b)(2c)(3a)(3c)(4a)(4c) \\
&= \left[-j\sqrt{(1-\gamma)a_{11}}\right]\left[\sqrt{t_{11}}e^{j\phi_{11}}\right]\left[-j\sqrt{(1-\gamma)a_{21}}\right]\left[\sqrt{t_{12}}e^{j\phi_{12}}z^{-2}\right] \\
&\left[\sqrt{(1-\gamma)(1-a_{12})}\right]\left[\sqrt{t_{22}}e^{j\phi_{22}}z^{-1}\right]\left[\sqrt{(1-\gamma)(1-a_{22})}\right] \\
&= -(1-\gamma)^2\sqrt{a_{11}a_{21}(1-a_{12})(1-a_{22})t_{11}t_{12}t_{22}}e^{j(\phi_{11}+\phi_{12}+\phi_{22})}z^{-3}
\end{aligned}
\qquad \text{Eq. 29}
$$

$$
\begin{aligned}
P_3 &= (1a)(1d)(2b)(2c)(3a)(3d)(4b)(4c) \\
&= \left[-j\sqrt{(1-\gamma)a_{11}}\right]\left[\sqrt{t_{11}}e^{j\phi_{11}}\right]\left[-j\sqrt{(1-\gamma)a_{21}}\right]\left[\sqrt{t_{12}}e^{j\phi_{12}}z^{-2}\right] \\
&\left[-j\sqrt{(1-\gamma)a_{12}}\right]\left[\sqrt{t_{12}}e^{j\phi_{12}}\right]\left[-j\sqrt{(1-\gamma)a_{22}}\right] \\
&= (1-\gamma)^2\sqrt{a_{11}a_{21}a_{12}a_{22}t_{11}}t_{12}e^{j(2\phi_{12}+\phi_{11})}z^{-2}
\end{aligned}
\qquad \text{Eq. 30}
$$

$$
\begin{aligned}
P_4 &= (1a)(1c)(2a)(2d)(3b)(3c)(4a)(4c) \\
&= \left[\sqrt{(1-\gamma)(1-a_{11})}\right]\left[\sqrt{t_{21}}e^{j\phi_{21}}z^{-2}\right]\left[-j\sqrt{(1-\gamma)a_{21}}\right]\left[\sqrt{t_{21}}e^{j\phi_{21}}\right] \\
&\left[-j\sqrt{(1-\gamma)a_{12}}\right]\left[\sqrt{t_{22}}e^{j\phi_{22}}z^{-1}\right]\left[\sqrt{(1-\gamma)(1-a_{22})}\right] \\
&= -(1-\gamma)^2\sqrt{(1-a_{11})a_{21}a_{12}(1-a_{22})t_{22}}t_{21}e^{j(2\phi_{21}+\phi_{22})}z^{-3}
\end{aligned}
\qquad \text{Eq. 31}
$$

$$
\begin{aligned}
P_5 &= (1a)(1c)(2a)(2c)(3a)(3d)(4b)(4c) \\
&= \left[\sqrt{(1-\gamma)(1-a_{11})}\right]\left[\sqrt{t_{21}}e^{j\phi_{21}}z^{-2}\right]\left[\sqrt{(1-\gamma)(1-a_{21})}\right]\left[\sqrt{t_{12}}e^{j\phi_{12}}z^{-2}\right] \\
&\left[-j\sqrt{(1-\gamma)a_{12}}\right]\left[\sqrt{t_{12}}e^{j\phi_{12}}\right]\left[-j\sqrt{(1-\gamma)a_{22}}\right] \\
&= -(1-\gamma)^2\sqrt{(1-a_{11})(1-a_{21})a_{12}a_{22}t_{21}}t_{12}e^{j(2\phi_{12}+\phi_{21})}z^{-4}
\end{aligned}
\qquad \text{Eq. 32}
$$

Hence, by substituting the Manson's gain transfer, the transfer function of bar function is yielded as below.

$$
\begin{aligned}
P_{bar2} &= (1-\gamma)^2\sqrt{(1-a_{11})(1-a_{21})(1-a_{12})(1-a_{22})t_{21}t_{12}r_{22}}e^{j(\phi_{21}+\phi_{12}+\phi_{22})}z^{-5} \\
&-(1-\gamma)^2\sqrt{(1-a_{11})(1-a_{21})a_{12}a_{22}t_{21}}t_{12}e^{j(2\phi_{12}+\phi_{21})}z^{-4} \\
&-(1-\gamma)^2\sqrt{a_{11}a_{21}(1-a_{12})(1-a_{22})t_{11}t_{12}t_{22}}e^{j(\phi_{11}+\phi_{12}+\phi_{22})}z^{-3} \\
&-(1-\gamma)^2\sqrt{(1-a_{11})a_{21}a_{12}(1-a_{22})t_{22}}t_{21}e^{j(2\phi_{21}+\phi_{22})}z^{-3} \\
&+(1-\gamma)^2\sqrt{a_{11}a_{21}a_{12}a_{22}t_{11}}t_{12}e^{j(2\phi_{12}+\phi_{11})}z^{-2} \\
&= (1-\gamma)^2\sqrt{(1-a_{11})(1-a_{21})(1-a_{12})(1-a_{22})t_{21}t_{12}r_{22}}e^{j(\phi_{21}+\phi_{12}+\phi_{22})}z^{-5} \\
&-(1-\gamma)^2\sqrt{(1-a_{11})(1-a_{21})a_{12}a_{22}t_{21}}t_{12}e^{j(2\phi_{12}+\phi_{21})}z^{-4} \\
&-(1-\gamma)^2\sqrt{a_{21}(1-a_{22})t_{22}}e^{j\phi_{22}}\left[\sqrt{a_{11}(1-a_{12})t_{11}t_{12}}e^{j(\phi_{11}+\phi_{12})}+\sqrt{(1-a_{11})a_{12}}t_{21}e^{j2\phi_{21}}\right]z^{-3} \\
&+(1-\gamma)^2\sqrt{a_{11}a_{21}a_{12}a_{22}t_{11}}t_{12}e^{j(2\phi_{12}+\phi_{11})}z^{-2}
\end{aligned}
\qquad \text{Eq. 33}
$$

- *Transfer function of the cross function*

The transfer function of the cross function is taking from the input port 1a to the output port 4d. Similarly because there is no feed-back loop existing in this system. Thus, the transfer function of the cross function now just depends on the numerator which is the summation of all path gains in this case.

There are 5 paths to go from input port 1a to output port 4d which correspond to the following path gains.

$$\begin{aligned}
P_1 &= (1a)(1c)(2a)(2c)(3a)(3c)(4a)(4d) \\
&= \left[\sqrt{(1-\gamma)(1-a_{11})}\sqrt{t_{21}}e^{j\phi_{21}}z^{-2}\sqrt{(1-\gamma)(1-a_{21})}\sqrt{t_{12}}e^{j\phi_{12}}z^{-2}\right] \\
&\left[\sqrt{(1-\gamma)(1-a_{12})}\sqrt{t_{22}}e^{j\phi_{22}}z^{-1}\left[-j\sqrt{(1-\gamma)a_{22}}\right]\right] \\
&= -j(1-\gamma)^2\sqrt{(1-a_{11})(1-a_{21})(1-a_{12})a_{22}t_{21}t_{12}t_{22}}e^{j(\phi_{21}+\phi_{12}+\phi_{22})}z^{-5}
\end{aligned} \qquad \text{Eq. 34}$$

$$\begin{aligned}
P_2 &= (1a)(1d)(2b)(2c)(3a)(3c)(4a)(4d) \\
&= \left[-j\sqrt{(1-\gamma)a_{11}}\sqrt{t_{11}}e^{j\phi_{11}}\left[-j\sqrt{(1-\gamma)a_{21}}\right]\sqrt{t_{12}}e^{j\phi_{12}}z^{-2}\right] \\
&\left[\sqrt{(1-\gamma)(1-a_{12})}\sqrt{t_{22}}e^{j\phi_{22}}z^{-1}\left[-j\sqrt{(1-\gamma)a_{22}}\right]\right] \\
&= -(1-\gamma)^2\sqrt{a_{11}a_{21}(1-a_{12})a_{22}t_{11}t_{12}t_{22}}e^{j(\phi_{11}+\phi_{12}+\phi_{22})}z^{-3}
\end{aligned} \qquad \text{Eq. 35}$$

$$\begin{aligned}
P_3 &= (1a)(1d)(2b)(2c)(3a)(3d)(4b)(4d) \\
&= \left[-j\sqrt{(1-\gamma)(1-a_{11})}\sqrt{t_{11}}e^{j\phi_{11}}\left[-j\sqrt{(1-\gamma)a_{21}}\right]\sqrt{t_{12}}e^{j\phi_{12}}z^{-2}\right] \\
&\left[-j\sqrt{(1-\gamma)a_{12}}\sqrt{t_{12}}e^{j\phi_{12}}\sqrt{(1-\gamma)(1-a_{22})}\right] \\
&= j(1-\gamma)^2\sqrt{(1-a_{11})a_{21}a_{12}(1-a_{22})t_{11}}t_{12}e^{j(2\phi_{12}+\phi_{11})}z^{-2}
\end{aligned} \qquad \text{Eq. 36}$$

$$\begin{aligned}
P_4 &= (1a)(1c)(2a)(2d)(3b)(3c)(4a)(4d) \\
&= \left[\sqrt{(1-\gamma)(1-a_{11})}\sqrt{t_{21}}e^{j\phi_{21}}z^{-2}\left[-j\sqrt{(1-\gamma)a_{21}}\right]\left[\sqrt{t_{21}e^{j\phi_{21}}}\right]\right] \\
&\left[-j\sqrt{(1-\gamma)a_{12}}\sqrt{t_{22}}e^{j\phi_{22}}z^{-1}\left[-j\sqrt{(1-\gamma)a_{22}}\right]\right] \\
&= j(1-\gamma)^2\sqrt{(1-a_{11})a_{21}a_{12}a_{22}t_{22}}t_{21}e^{j(2\phi_{21}+\phi_{22})}z^{-3}
\end{aligned} \qquad \text{Eq. 37}$$

$$\begin{aligned}
P_5 &= (1a)(1c)(2a)(2c)(3a)(3d)(4b)(4d) \\
&= \left[\sqrt{(1-\gamma)(1-a_{11})}\sqrt{t_{21}}e^{j\phi_{21}}z^{-2}\sqrt{(1-\gamma)(1-a_{21})}\sqrt{t_{12}}e^{j\phi_{12}}z^{-2}\right] \\
&\left[-j\sqrt{(1-\gamma)a_{12}}\sqrt{t_{12}}e^{j\phi_{12}}\sqrt{(1-\gamma)(1-a_{22})}\right] \\
&= -j(1-\gamma)^2\sqrt{(1-a_{11})(1-a_{21})a_{12}(1-a_{22})t_{21}}t_{12}e^{j(2\phi_{12}+\phi_{21})}z^{-4}
\end{aligned} \qquad \text{Eq. 38}$$

Hence, transfer function of the cross function is the sum of all 5 different path gains from P_1 through P_5.

$$
\begin{aligned}
P_{cross2} &= -j(1-\gamma)^2\sqrt{(1-a_{11})(1-a_{21})(1-a_{12})a_{22}t_{21}t_{12}t_{22}}\,e^{j(\phi_{21}+\phi_{12}+\phi_{22})}z^{-5} \\
&- j(1-\gamma)^2\sqrt{(1-a_{11})(1-a_{21})a_{12}(1-a_{22})t_{21}}\,t_{12}e^{j(2\phi_{12}+\phi_{21})}z^{-4} \\
&-(1-\gamma)^2\sqrt{a_{11}a_{21}(1-a_{12})a_{22}t_{11}t_{12}t_{22}}\,e^{j(\phi_{11}+\phi_{12}+\phi_{22})}z^{-3} \\
&+ j(1-\gamma)^2\sqrt{(1-a_{11})a_{21}a_{12}a_{22}t_{22}}\,t_{21}e^{j(2\phi_{21}+\phi_{22})}z^{-3} \\
&+(1-\gamma)^2\sqrt{(1-a_{11})a_{21}a_{12}(1-a_{22})t_{11}}\,t_{12}e^{j(2\phi_{12}+\phi_{11})}z^{-2} \\
&= -j(1-\gamma)^2\sqrt{(1-a_{11})(1-a_{21})(1-a_{12})a_{22}t_{21}t_{12}t_{22}}\,e^{j(\phi_{21}+\phi_{12}+\phi_{22})}z^{-5} \\
&- j(1-\gamma)^2\sqrt{(1-a_{11})(1-a_{21})a_{12}(1-a_{22})t_{21}}\,t_{12}e^{j(2\phi_{12}+\phi_{21})}z^{-4} \\
&-(1-\gamma)^2\sqrt{a_{21}a_{22}t_{22}}\,e^{j(\phi_{22})}\left[\sqrt{a_{11}(1-a_{12})t_{11}t_{12}}\,e^{j(\phi_{11}+\phi_{12})} - j\sqrt{(1-a_{11})a_{12}}\,t_{21}e^{j2\phi_{21}}\right]z^{-3} \\
&+(1-\gamma)^2\sqrt{(1-a_{11})a_{21}a_{12}(1-a_{22})t_{11}}\,t_{12}e^{j(2\phi_{12}+\phi_{11})}z^{-2}
\end{aligned}
\qquad \text{Eq. 39}
$$

2.4.2.4 Simulation results

Similarly to the case of N = 2, the optical FIR HBF when the number of interferometers is three is considered by observing the roots locations of the zeros, and the frequency responses of the transfer functions of the cross and bar functions as illustrated in *Figure 15* to *Figure 16*.

In the case of three interferometers (i.e. N = 3), there are 3 zeros and 3 poles (at the origin) in the system. For ideal condition, as mentioned in the introduction all calculations had been done in the case of no loss (i.e. $\gamma = 0\%$). By using MATLAB simulation, roots locations and frequency response have been carried out as follow.

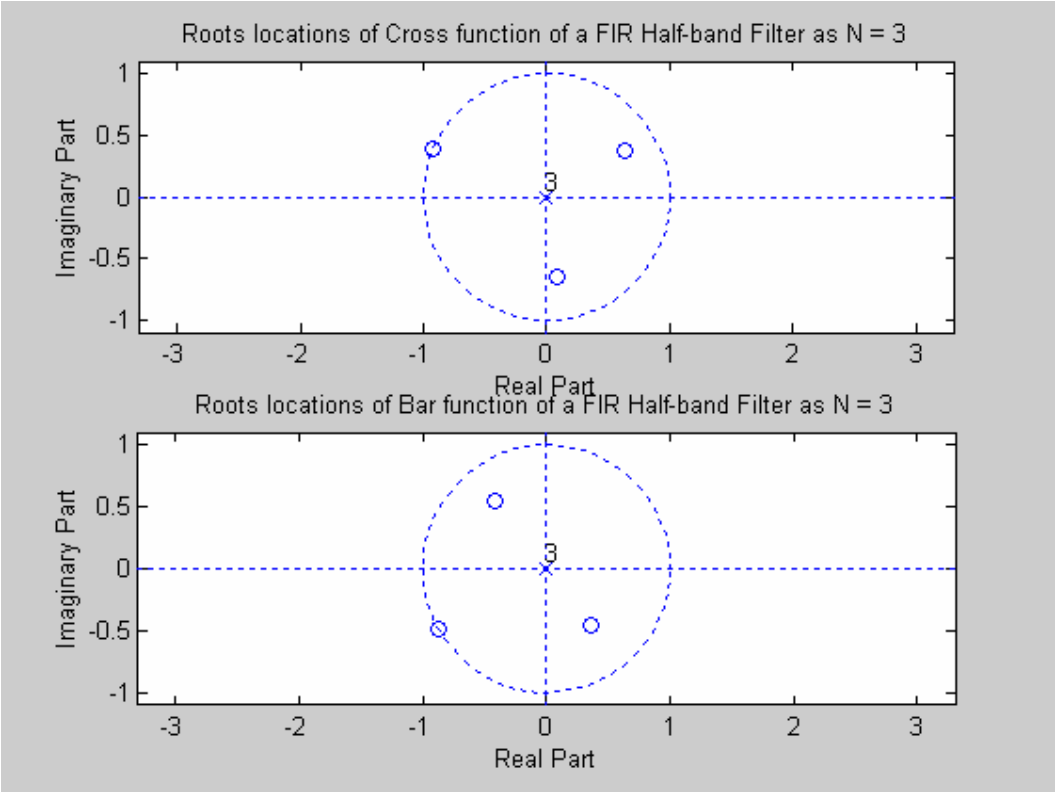

Figure 15: The optical FIR HBF length-3: the roots locations of the transfer functions.

As shown in *Figure 15*, the MATLAB simulation had been taken and derived the best locations for zeros where 3 zeros had been taken as near the unit circle as they can to observe the best linear phase.

In order to satisfy the stability of the system, the chosen values for optical phase shifts, intensity transmission coefficients as well as intensity coupling coefficients are set. The Table 3 and Table 4shows the chosen values of the bar and the cross transfer function respectively.

Intensity coupling coefficients (a_{pq})			
a_{11}	a_{12}	a_{21}	a_{22}
0.5	0.6	0.5	3
Intensity transmission coefficients (t_{pq})			
t_{11}	t_{12}	t_{21}	t_{22}
21	4.5	3	11
Optical phase shift (Φ_{pq})			
ϕ_{11}	ϕ_{12}	ϕ_{21}	ϕ_{22}
π	$\pi/4$	$\pi/3$	π

Table 3: Optical FIR HBF when N = 3: The chosen parameters of the transfer function of the bar function.

Intensity coupling coefficients (a_{pq})			
a_{11}	a_{12}	a_{21}	a_{22}
0.3	0.15	0.3	0.05
Intensity transmission coefficients (t_{pq})			
t_{11}	t_{12}	t_{21}	t_{22}
12	1.2	3	11
Optical phase shift (Φ_{pq})			
ϕ_{11}	ϕ_{12}	ϕ_{21}	ϕ_{22}
π	$\pi/4$	$\pi/3$	Π

Table 4*: Optical FIR HBF when N = 3: The chosen parameters of the transfer function of the cross function.*

The magnitude responses and phase responses of the transfer functions of the bar and the cross functions are shows in *Figure 16* and *Figure 17* respectively.

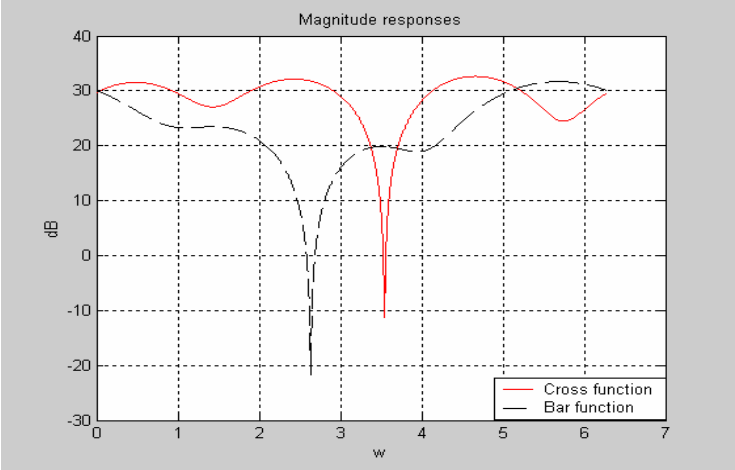

Figure 16: The optical FIR HBF length-3: the magnitude responses.

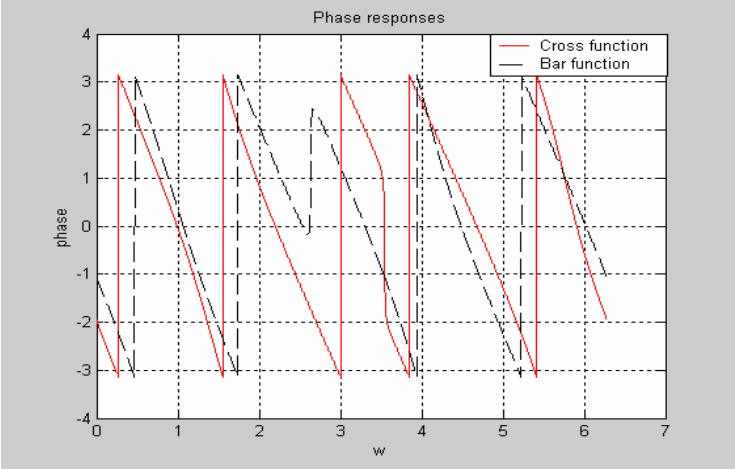

Figure 17: The optical FIR HBF length-3: the phase responses.

Figure 17 shows in their magnitude responses where there is the energy of the bar function pulls up, that of the cross function pulls down. Although their phase responses did not achieve the exact linear phase, they still show the linear phase in such long periods.

In this case when the optical FIR HBFlength-3 is considered, the frequency responses with respected to the transfer function of the cross and the bar functions are having the same property. Thus, after the transmission the light-wave from either output 4c or 4d can be removed.

2.5 Optical IIR half-ban Filters

If the FIR filters are famous because of the exact linear phases that they can achieve, the IIR filters can be ideal for those who want a very short transition from pass-band to stop-band. This is achieved by the combination of a pole near the unit circle and a zero near the unit circle. As mentioned earlier, the multi-rate signal processing systems are attracted by HBF since it provides the great opportunity to down-sampling wherever the signals needs to convert to.

The main difference between the FIR and IIR HBF is whether the coupler had some feed-back or not. As studied in the previous part, FIR HBFs were all about straight forward waveguides, so, in this part, IIR HBF is going to take the feed-back from the output of the coupler to the other input coupler. In this Section, before study about optical IIR HBFs, the simplified ring-waveguides with double the path length difference are considered. It provides the simplest case of the optical IIR filter.

2.5.1 The Design Techniques of the Optical IIR HBFs

Figure 18 below shows the schematic diagram of the optical IIR HBF where transmission coefficients are indicated along the signal flow paths.

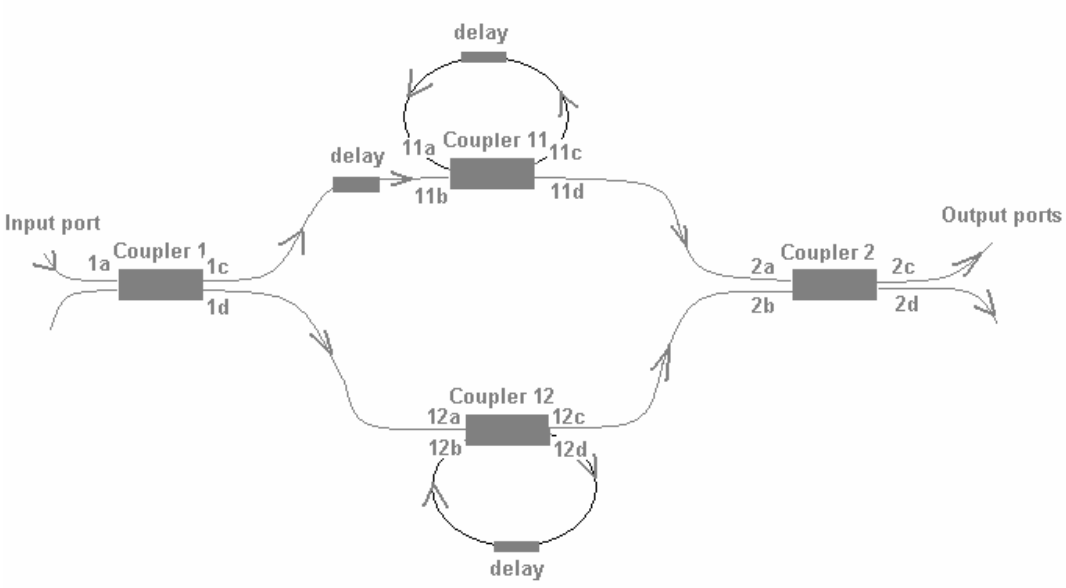

Figure 18: The schematic diagram of the optical IIR HBF.

The introduction to OFs, IIR filters characterize by their poles' and zeros' locations which lie within the unit circle in order to satisfy the stability of the systems. *Figure 18* above shows the schematic diagram of the optical IIR HBFs in the simplest case. Following the SFG paths, the designs of the poles and zeros are represented by the upper and the lower paths. In fact, pole and zero are described by cascading double-coupler feed-back optical resonators (DCFBOR). The delay shows in the top of each DCFFOR determines how many path length differences between two arms of an MZI. The delay located between the output port of coupler 1 (1c) and the input of coupler 11 (11a) characterizes the odd-order optical IIR HBFs when it set at 1.

In the next section the design of the optical IIR filter by cascading ring-waveguides with path length differences of 2ΔL. In this case, the delays those locate in DCFFORs are designed with path length differences of 2ΔL. The order delay that locates outside the ring-waveguide is neglected. The circuit configuration of this particular case is shown in *Figure 19*.

The last section describes the technical design of a fifth-order optical IIR HBF. Similar to the design technique of the optical FIR HBFs, the circuit configuration is converted into its SFG representation where every sign flow paths are indicated. The characteristics of the system are

characterized by the transfer functions of the bar and cross functions. Finally, the comment of which output light-wave can be chosen to give the sharper figure of optical HBF is discussed.

2.5.2 The Characteristics and Transfer functions of the Ring-waveguide Filter

The circuit configuration of an optical IIR filter is designed by cascading ring –waveguides. Using couples of 2 × 2 optical directional couplers, this circuit configuration which is illustrated below in figure 6.13 consists of MZI whose two arms are connected with ring-waveguides with path length differences of 2ΔL.

2.5.2.1 The circuit configurations of the ring-waveguide filter when the path length difference is 2ΔL

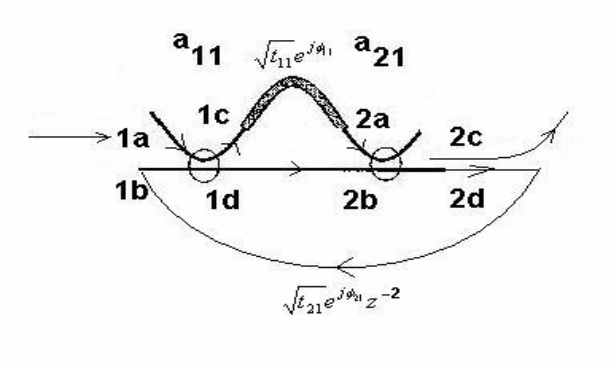

Figure 19: The schematic diagram of the optical IIR filter.

Figure 20 below shows the corresponding SFG Representation of *Figure 19* where transmission coefficients are indicated along the signal flow paths as follow.

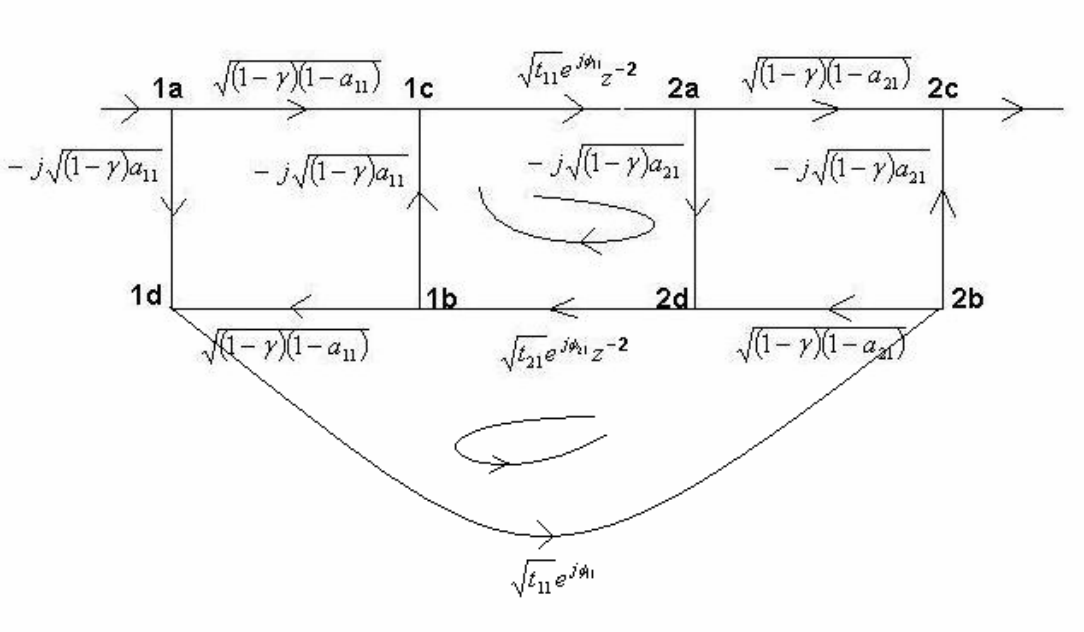

Figure 20:The SFG Representation of the optical IIR filter.

From the above SFG representation, the transfer functions of the bar and cross functions are calculated using the Manson's rule gain formula. The transfer function of the bar function is calculated by observing the ratio between the input power at the light-wave input port 1a and the output port 2c. That of the cross function is yielded by taking the relationship between the input power at the light-wave input port 1a and the output port 2d.

2.5.2.2 The transfer functions of the ring-waveguide filter

For ideal situation, the intensity coupling loss had been set to be zero. Unlike the cases of the optical FIR HBFs, optical IIR filters are designed by combined poles and zeros characteristics. By applying the Manson's rule gain to yield the transfer functions, the denominators are calculated by taking the factors of ∑(1 – Loop gains). *Figure 19* shows that there are two loops where their loop gains are valued as follow.

$$L_1 = -\sqrt{a_{11}a_{21}t_{11}t_{21}}e^{j(\phi_{11}+\phi_{21})}z^{-4}$$
$$L_2 = \sqrt{(1-a_{11})(1-a_{21})t_{11}t_{21}}e^{j(\phi_{11}+\phi_{21})}z^{-2} \qquad \text{Eq. 40}$$

Again following the SFG method, the denominator is calculated by observing the delta as follows.

Since the factors of ∑(1 – Loop gains) = $(1-L_1)(1-L_2)$; because L_1 touches L_2, every terms that consist L_1L_2 are cancelled and finally $\rightarrow \Delta = 1 - L_1 - L_2$; Substituting the values of these two loop gains L_1 and L_2, the denominator Δ is yielded as follows.

$$\Delta = 1 + \sqrt{a_{11}a_{21}t_{11}t_{21}}e^{j(\phi_{11}+\phi_{21})}z^{-4} - \sqrt{(1-a_{11})(1-a_{21})t_{11}t_{21}}e^{j(\phi_{11}+\phi_{21})}z^{-2} \qquad \text{Eq. 41}$$

This denominator Δ is calculated for the whole system. Hence, it is the denominator for both transfer functions of the bar and the cross functions. Manson's gain rule states that the transfer functions of the bar and cross functions now depend on the path gains that take from the path ways from input light-wave 1a to output port 2c and 2d respectively and their own determinants Δ_1 and Δ_2. However because two loops $L_1$and L_2 touch each other, the transfer functions only depend on their path gains.

- *Transfer function of the bar function*

Since there are two path ways where direct light-wave can go through from input 1a to output 2c, the transfer function of bar function is the sum of these two corresponding path gains whose are noted as P_1 and P_2 as follow.

$$P_1 = \sqrt{(1-a_{11})(1-a_{21})t_{11}}e^{j\phi_{11}}z^{-2}$$
$$P_2 = -\sqrt{a_{11}a_{21}t_{11}}e^{j\phi_{11}}$$

As discussed earlier, the transfer function of the bar function has the nominator which is the summation of the above path gains and the denominator which is calculated as delta Δ. Hence, Manson's gain can be substituted as follows.

$$H_b = \frac{\sqrt{(1-a_{11})(1-a_{21})t_{11}}e^{j\phi_{11}}z^{-2} - \sqrt{a_{11}a_{21}t_{11}}e^{j\phi_{11}}}{1 + \sqrt{a_{11}a_{21}t_{11}t_{21}}e^{j(\phi_{11}+\phi_{21})}z^{-4} - \sqrt{(1-a_{11})(1-a_{21})t_{11}t_{21}}e^{j(\phi_{11}+\phi_{21})}z^{-2}} \qquad \text{Eq. 42}$$

- *Transfer function of the cross function*

Because there are two path ways that allow the light-wave to go from input port 1a to output port 2d, the transfer function of a cross function is derived by summing two corresponding path gains whose value are calculated as follow.

$$P_1 = \left[-j\sqrt{a_{11}}\right]\left[\sqrt{t_{11}}e^{j\phi_{11}}\right]\left[\sqrt{(1-a_{21})}\right] = -j\sqrt{a_{11}(1-a_{21})t_{11}}e^{j\phi_{11}}$$
$$P_2 = \left[\sqrt{(1-a_{11})}\right]\left[\sqrt{t_{11}}e^{j\phi_{11}}z^{-2}\right]\left[-j\sqrt{a_{21}}\right] = -j\sqrt{(1-a_{11})a_{21}t_{11}}e^{j\phi_{11}}z^{-2} \quad \text{Eq. 43}$$

Thus, the transfer function of cross function is:

$$H_c = \frac{-j\sqrt{a_{11}(1-a_{21})t_{11}}e^{j\phi_{11}} - j\sqrt{(1-a_{11})a_{21}t_{11}}e^{j\phi_{11}}z^{-2}}{1+\sqrt{a_{11}a_{21}t_{11}t_{21}}e^{j(\phi_{11}+\phi_{21})}z^{-4} - \sqrt{(1-a_{11})(1-a_{21})t_{11}t_{21}}e^{j(\phi_{11}+\phi_{21})}z^{-2}} \quad \text{Eq. 44}$$

2.5.2.3 Simulation results

The MATLAB simulations are carried out to study the characteristics of the optical IIR filters via their transfer functions of the cross and bar functions. Unlike the technical design of the optical FIR HBFs, because of the effect of the feed-back loops and the touching loops, the characteristics of optical IIR filters are made.

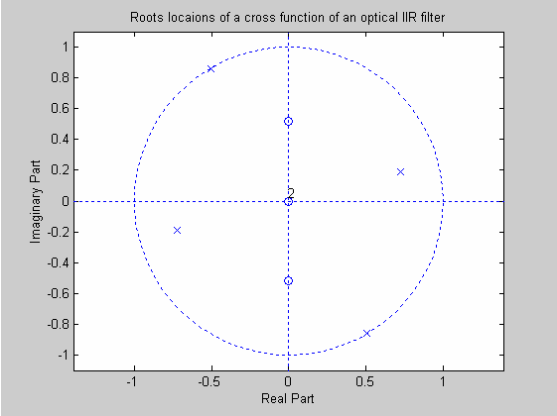

Figure 21: The Roots locations of a transfer function of the cross function of the optical IIR filter.

Because the path length differences which connected between two arms of the DCFFORs are set at 2ΔL, the result at the transfer function of the bar function as shown in *Figure 21* above is 4 poles and 4 zeros. They consist of 2 zeros at the origin, 2 other conjugated zeros and 2 pairs of conjugated poles.

The chosen values of optical phase shifts, intensity coupling coefficients and intensity transmission coefficients are listed in the Table 5 below. These assured that the stability of the

system is satisfied, and furthermore, the best option for poles that stay as near the unit circle as they can is made.

Intensity Coupling Coefficients (a_{pq})	
a_{11}	a_{21}
0.78	0.2
Intensity transmission coefficients (t_{pq})	
t_{11}	t_{21}
1	2
Optical phase shift (ϕ_{pq})	
ϕ_{11}	ϕ_{21}
π	$\pi/2$

Table 5: Optical IIR filter: The chosen parameters of the transfer function of the cross function.

Figure 22 below illustrates the frequency responses of the transfer function of the cross function of the optical IIR filter.

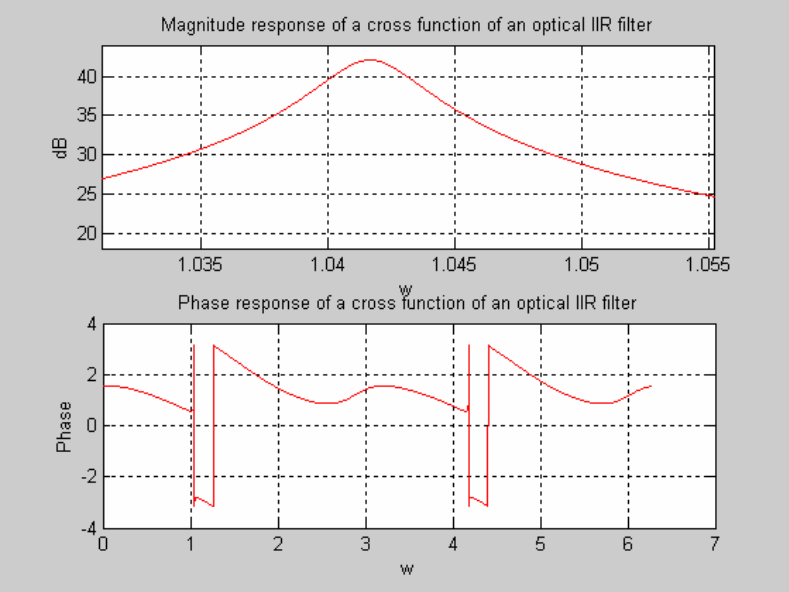

Figure 22: The Frequency Response of the transfer function of the cross function of the optical IIR filter.

As shown above, the maximum magnitude of the transfer function of the cross function is about 43 dB. The shape of the filter is made however; it is not sharp enough to give the ideal optical IIR filter. *Figure 23* illustrated the roots locations of the transfer function of the bar function of

the optical IIR filter. Similarly to that of the cross function, the fourth order optical IIR filter is done by cascading 4 poles and 4 zeros as shown below.

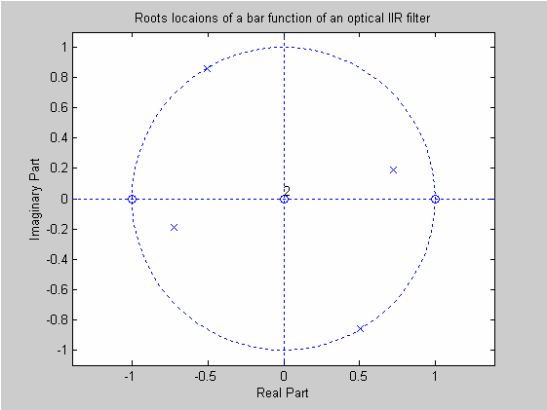

Figure 23: The Roots locations of the transfer function of the bar function of the optical IIR filter.

MATLAB simulation is done by taking these chosen values from the Table 6 as follows.

Intensity Coupling Coefficients (a_{pq})	
a_{11}	a_{21}
0.5	0.5
Intensity transmission coefficients (t_{pq})	
t_{11}	t_{21}
1	2
Optical phase shift (ϕ_{pq})	
ϕ_{11}	ϕ_{21}
π	$\pi/2$

Table 6: Optical IIR filter: The chosen parameters of the transfer function of the bar function.

Figure 24 describes the frequency responses of the transfer function of the bar function of the fourth order optical IIR filter.

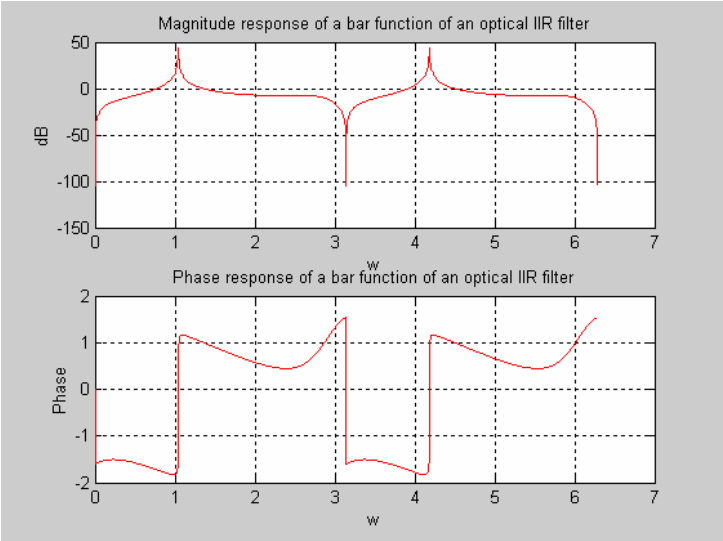

Figure 24: The Frequency Response of the transfer function of the bar function of the optical IIR filter.

Comparing to the magnitude response of the transfer function of the cross function, the magnitude of the transfer function of the bar function is clearly sharper. Furthermore the short transition from pass-band to stop-band is achieved. Thus, in order to design the fourth order optical IIR filter the output light-wave that takes from the output port 2c of the bar function is the one to observe or study at the end of the transmission.

2.5.3 The Characteristics and Transfer functions of the Fifth order Optical IIR HBFs

In this section, the optical IIR HBF and particular the corresponding fifth order system has been investigated. An optical IIR HBF can be designed by eliminating the Jinguji's *et al* [14] novel circuit configuration. This conventional configuration can be extended to circuit configurations with M upper-rings and N lower-rings in order to realize any arbitrary-order IIR HBF characteristics. In the next Sub-section, the simplest case when M = 1 and N = 1, that means number of ring waveguides had been set to minimum is observed.

The circuit configuration of the fifth order optical IIR HBF and its corresponding SFG representation are illustrated in *Figure 25* and *Figure 26* respectively.

2.5.3.1 The circuit configurations of the fifth order optical IIR HBF

The circuit configuration of the optical IIR HBF can be extracted from the schematic diagram of optical IIR HBF. As mentioned peviously, for the simplest case, number of the ring-waveguides in the upper-rings and lower-rings are equal to 1 (M = N = 1), it is the case of the fifth order optical IIR HBF. The corresponding circuit configuration consists of an MZI whose two arms are connected with a number of ring-waveguides with a path length difference of 2ΔL. And the path length difference between two arms, which means between the output port 1c and input port 11a of the upper-ring, is ΔL. It is illustrated in the *Figure 25*.

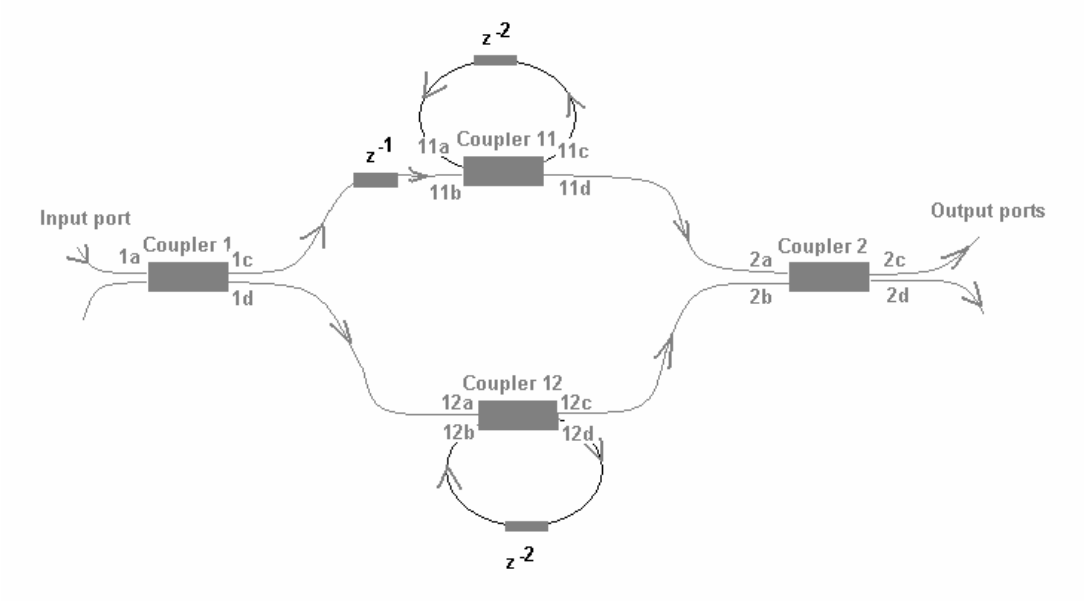

Figure 25: The schematic diagram of the fifth order optical IIR HBF.

The corresponding SFG is shown in *Figure 26* which indicates two independent ring-waveguides in order to form poles and zeros of the system.

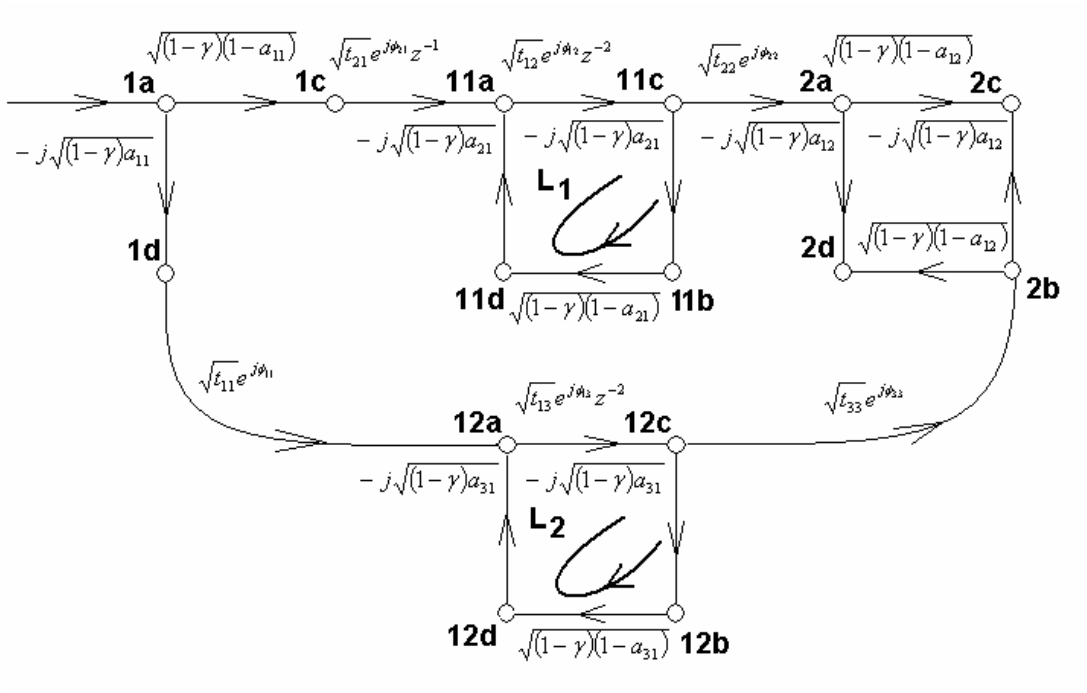

Figure 26: The SFG Representation of the fifth order optical IIR HBF.

2.5.3.2 The transfer functions of the fifth order optical IIR filter

Figure 26 shows that there are 2 loops in this system whose loop gains are denoted as L_1 through L_2 as follow.

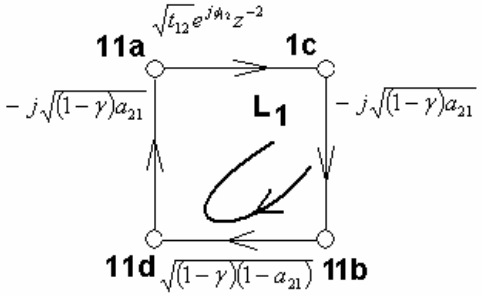

$$L_1 = -(1-\gamma)\sqrt{(1-\gamma)(1-a_{21})t_{12}}\,a_{21}e^{j\phi_{12}}z^{-2}$$

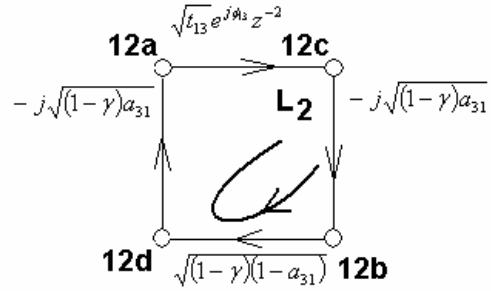

$$L_2 = -(1-\gamma)\sqrt{(1-\gamma)(1-a_{31})t_{13}}\,a_{31}e^{j\phi_{31}}z^{-2}$$

Figure 27*: The loop gains' representations of the fifth order optical IIR HBF.*

For ideal condition, the intensity coupling loss had been set at 0%. By applying the Manson's rule gain to yield the transfer functions, the denominators are calculated by taking the factors of ∑(1 – Loop gains) as follow.

$$\begin{aligned}&(1-L_1)(1-L_2)\\&=1-(L_1+L_2)+(L_1L_2)\end{aligned} \qquad \text{Eq. 45}$$

Besides, loop L_1 does not touch L_2 hence

$$\begin{aligned}&\Delta=1-(L_1+L_2)+(L_1L_2)\\&=1+\left(\sqrt{(1-a_{21})t_{12}}\,a_{21}e^{j\phi_{12}}+\sqrt{(1-a_{31})t_{13}}\,a_{31}e^{j\phi_{13}}\right)z^{-2}+\left(\sqrt{(1-a_{21})(1-a_{31})t_{12}t_{13}}\,a_{21}a_{31}e^{j(\phi_{12}+\phi_{31})}\right)z^{-4}\end{aligned} \qquad \text{Eq. 46}$$

This denominator Δ is calculated for the whole system. Hence, it is the denominator for both transfer functions of the bar and the cross functions. Manson's gain rule and Equation 2.6 states that the transfer functions of the bar and cross functions now depend on the path gains that take from the path ways from input light-wave 1a to output port 2c and 2d respectively. And the transfer functions of the cross and bar functions are calculated as follow.

- *Transfer function of the bar function*

Transfer function of the bar function is taken from the input 1a through the output 2c. Because there are 2 path ways that allow the light power goes through 1a to 2c, the Manson's gain rule [Equation 2.6] states that the denominator of the transfer function of the bar function is the summation of these two corresponding path gains P_1 and P_2 and their own determinants Δ_1 and Δ_2 as follow.

$$\begin{aligned}&P_1=\sqrt{(1-a_{11})(1-a_{12})t_{21}t_{12}t_{22}}\,e^{j(\phi_{12}+\phi_{21}+\phi_{22})}z^{-3}\\&\Delta_1=1-L_2\\&\rightarrow P_1\Delta_1=\sqrt{(1-a_{11})(1-a_{12})t_{12}t_{21}t_{22}}\,e^{j(\phi_{12}+\phi_{21}+\phi_{22})}z^{-3}\\&+\sqrt{(1-a_{11})(1-a_{12})(1-a_{31})t_{12}t_{21}t_{22}t_{13}}\,a_{31}e^{j(\phi_{12}+\phi_{21}+\phi_{22}+\phi_{13})}z^{-5}\end{aligned} \qquad \text{Eq. 47}$$

$$
\begin{aligned}
&P_2 = -\sqrt{a_{11}a_{12}t_{11}t_{13}t_{33}}\,e^{j(\phi_{11}+\phi_{13}+\phi_{33})}z^{-2} \\
&\Delta_2 = 1 - L_1 \\
&\rightarrow P_2\Delta_2 = -\sqrt{a_{11}a_{12}t_{11}t_{13}t_{33}}\,e^{j(\phi_{11}+\phi_{13}+\phi_{33})}z^{-2} \\
&-\sqrt{(1-a_{21})a_{11}a_{12}t_{11}t_{12}t_{13}t_{33}}\,a_{21}e^{j(\phi_{11}+\phi_{12}+\phi_{13}+\phi_{33})}z^{-4}
\end{aligned}
\qquad \text{Eq. 48}
$$

The transfer function of the bar function is calculated as follows.

$$H_{cross} = \frac{\sum_{i=1}^{N} P_i\Delta_1}{\Delta} = \frac{\mathrm{Num}_{\mathrm{cross}}}{\Delta}$$

where

$$
\begin{aligned}
&\mathrm{Num}_{\mathrm{cross}} = -\sqrt{a_{11}a_{12}t_{11}t_{13}t_{33}}\,e^{j(\phi_{11}+\phi_{13}+\phi_{33})}z^{-2} + \sqrt{(1-a_{11})(1-a_{12})t_{12}t_{21}t_{22}}\,e^{j(\phi_{12}+\phi_{21}+\phi_{22})}z^{-3} \\
&-\sqrt{(1-a_{21})a_{11}a_{12}t_{11}t_{12}t_{13}t_{33}}\,a_{21}e^{j(\phi_{11}+\phi_{12}+\phi_{13}+\phi_{33})}z^{-4} + \sqrt{(1-a_{11})(1-a_{12})(1-a_{31})t_{12}t_{21}t_{22}t_{13}}\,a_{31}e^{j(\phi_{12}+\phi_{21}+\phi_{22}+\phi_{13})}z^{-5} \\
&\Delta = 1-(L_1+L_2)+(L_1L_2) \\
&= 1+\left(\sqrt{(1-a_{21})t_{12}}\,a_{21}e^{j\phi_{12}} + \sqrt{(1-a_{31})t_{13}}\,a_{31}e^{j\phi_{13}}\right)z^{-2} + \left(\sqrt{(1-a_{21})(1-a_{31})t_{12}t_{13}}\,a_{21}a_{31}e^{j(\phi_{12}+\phi_{31})}\right)z^{-4}
\end{aligned}
\qquad \text{Eq. 49}
$$

- *Transfer function of the cross function*

The transfer function of the cross function is taken from the input 1a through the output 2d. Similarly, there are 2 path ways to let the light power goes through 1a to 2d whose corresponding path gains and the factors of $P_i\Delta_i$ are calculated below.

$$
\begin{aligned}
&P_1 = -j\sqrt{(1-a_{11})a_{21}t_{21}t_{12}t_{22}}\,e^{j(\phi_{12}+\phi_{21}+\phi_{22})}z^{-3} \\
&\Delta_1 = 1 - L_2 \text{ since it touches loop } \mathrm{L}_1 \\
&= 1+\sqrt{(1-a_{31})t_{13}}\,a_{13}e^{j\phi_{13}}z^{-2} \\
&\rightarrow P_1\Delta_1 = -j\sqrt{(1-a_{11})a_{12}t_{21}t_{12}t_{22}}\,e^{j(\phi_{12}+\phi_{21}+\phi_{22})}z^{-3} - j\sqrt{(1-a_{11})(1-a_{31})t_{12}t_{21}t_{22}t_{13}}\,a_{31}z^{-5}
\end{aligned}
\qquad \text{Eq. 50}
$$

$$
\begin{aligned}
&P_2 = -j\sqrt{(1-a_{12})a_{11}t_{11}t_{13}t_{33}}\,e^{j(\phi_{11}+\phi_{13}+\phi_{33})}z^{-2} \\
&\Delta_2 = 1 - L_1 \\
&= 1+\sqrt{(1-a_{21})t_{12}}\,a_{21}z^{-2} \\
&\rightarrow P_2\Delta_2 = -j\sqrt{(1-a_{12})a_{11}t_{11}t_{13}t_{33}}\,e^{j(\phi_{11}+\phi_{13}+\phi_{33})}z^{-2} - j\sqrt{(1-a_{12})(1-a_{21})a_{11}t_{11}t_{12}t_{13}t_{33}}\,a_{21}e^{j(\phi_{11}+\phi_{12}+\phi_{13}+\phi_{33})}z^{-4}
\end{aligned}
\qquad \text{Eq. 51}
$$

Substituting Equation 2.9, the transfer function of the bar function is calculated as follows.

$$H_{cross} = \frac{\sum_{i=1}^{N} P_i \Delta_1}{\Delta} = \frac{\mathrm{Num}_{\mathrm{cross}}}{\Delta}$$

where

$$\mathrm{Num}_{\mathrm{cross}} = -j\sqrt{(1-a_{11})a_{12}t_{21}t_{12}t_{22}}\,e^{j(\phi_{12}+\phi_{21}+\phi_{22})}z^{-3} - j\sqrt{(1-a_{11})(1-a_{31})t_{12}t_{21}t_{22}t_{13}}\,a_{31}z^{-5} \qquad \text{Eq. 52}$$

$$- j\sqrt{(1-a_{12})a_{11}t_{11}t_{13}t_{33}}\,e^{j(\phi_{11}+\phi_{13}+\phi_{33})}z^{-2} - j\sqrt{(1-a_{12})(1-a_{21})a_{11}t_{11}t_{12}t_{13}t_{33}}\,a_{21}e^{j(\phi_{11}+\phi_{12}+\phi_{13}+\phi_{33})}z^{-4}$$

$$\Delta = 1-(L_1+L_2)+(L_1L_2)$$

$$= 1+\left(\sqrt{(1-a_{21})t_{12}}\,a_{21}e^{j\phi_{12}} + \sqrt{(1-a_{31})t_{13}}\,a_{31}e^{j\phi_{13}}\right)z^{-2} + \left(\sqrt{(1-a_{21})(1-a_{31})t_{12}t_{13}}\,a_{21}a_{31}e^{j(\phi_{12}+\phi_{31})}\right)z^{-4}$$

2.5.3.3 Simulation results

The MATLAB simulations are carried out to study the characteristics of the optical IIR filters via their transfer functions of the cross and bar functions as follow.

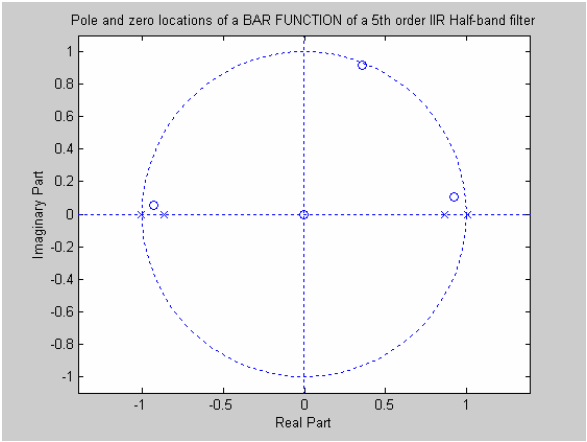

Figure 28: The Roots locations of the transfer function of the bar function of the fifth order optical IIR HBF.

Because the path length differences which connected between two arms of the DCFFORs are set at 2ΔL, and the delay that occurs between the output of port 1c and the input port 11a is z^{-1}; the result at the transfer function of the bar function as shown in *Figure 28* above is 5 poles and 4 zeros. The chosen values of optical phase shifts, intensity coupling coefficients and intensity transmission coefficients are listed in the *Table 7* below. These assured that the stability of the system is satisfied, and furthermore, the best option for poles that stay as near the unit circle as they can is made.

Intensity Coupling Coefficients (a_{pq})

a_{11}	a_{12}	a_{21}	a_{31}		
0.8	0.61	0.85	1		
Intensity Transmission Coefficients (t_{pq})					
t_{11}	t_{12}	t_{21}	t_{22}	t_{13}	t_{33}
40	8	10	2	9	2
Optical Phase Shift (ϕ_{pq})					
ϕ_{11}	ϕ_{12}	ϕ_{21}	ϕ_{22}	ϕ_{13}	ϕ_{33}
π/10	-π/2	-π/2	π	π/50	π

Table 7: The fifth order optical IIR HBF: The chosen parameters of the transfer function of the bar function.

Figure 29 below illustrates the frequency responses of the transfer function of the bar function of the fifth order optical IIR HBF.

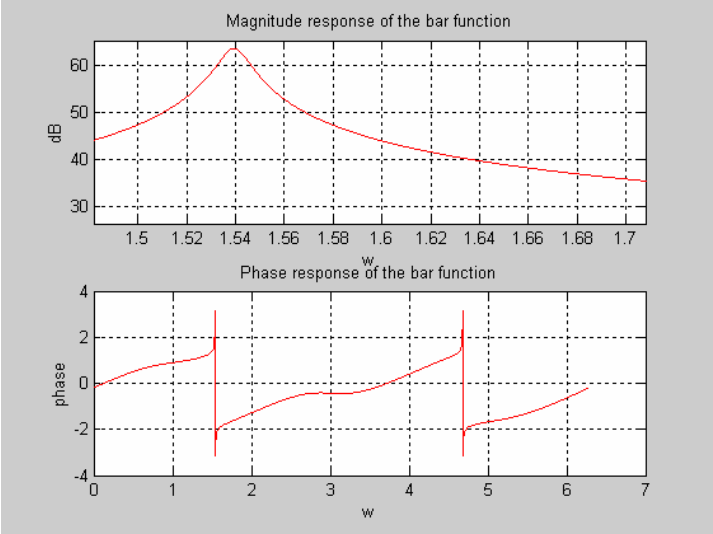

Figure 29: The Frequency Response of the transfer function of the bar function of the fifth order optical IIR HBF.

As shown above, the maximum magnitude of the transfer function of the bar function is about 63 dB. The shape of the filter is made however; it is not sharp enough to give the ideal optical IIR HBF.

Figure 30 illustrated the roots locations of the transfer function of the cross function of the fifth order optical IIR HBF. Similarly to that of the bar function, the fifth order optical IIR HBF is done by cascading 5 poles and 4 zeros as shown below.

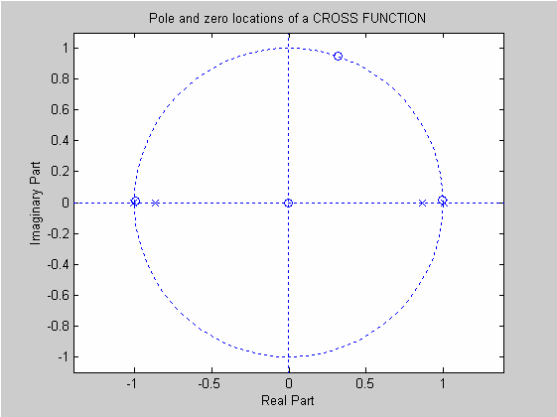

Figure 30: The Roots locations of the transfer function of the cross function of the fifth order optical IIR HBF.

MATLAB simulation is done by taking these chosen values from the table 6.8 as follows.

Intensity Coupling Coefficients (a_{pq})					
a_{11}	a_{12}	a_{21}	a_{31}		
0.25	0.61	0.8	0.3		
Intensity Transmission Coefficients (t_{pq})					
t_{11}	t_{12}	t_{21}	t_{22}	t_{13}	t_{33}
40	8	10	2	9	2
Optical Phase Shift (ϕ_{pq})					
ϕ_{11}	ϕ_{12}	ϕ_{21}	ϕ_{22}	ϕ_{13}	ϕ_{33}
$\pi/10$	π	$\pi/2$	π	π	π

Table 8: The fifth order optical IIR HBF: The chosen parameters of the transfer function of the cross function.

Figure 31 describes the frequency responses of the transfer function of the cross function of the fifth order optical IIR HBF.

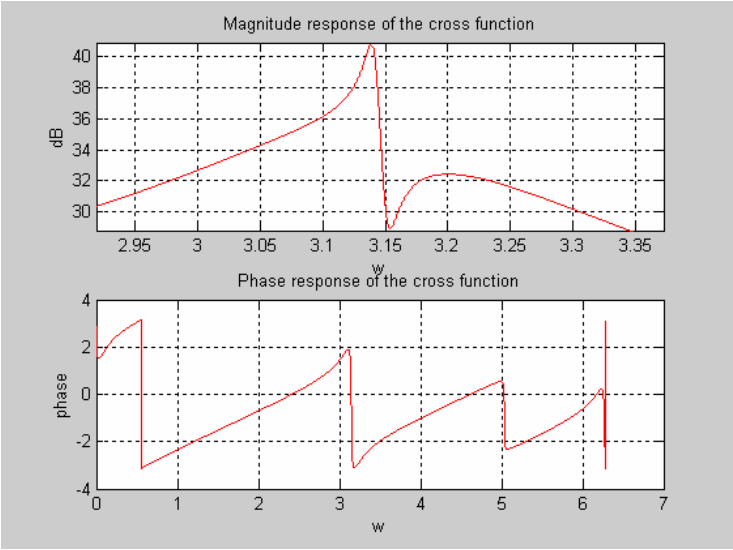

Figure 31: The Frequency Response of the transfer function of the cross function of the fifth order optical IIR HBF.

Comparing to the magnitude response of the transfer function of the bar function, the magnitude of the transfer function of the cross function is clearly sharper. Furthermore the short transition from pass-band to stop-band is achieved. Thus, in order to design the fifth order optical IIR HBF the output light-wave that takes from the output port 2c of the bar function is the one to observe or study at the end of the transmission.

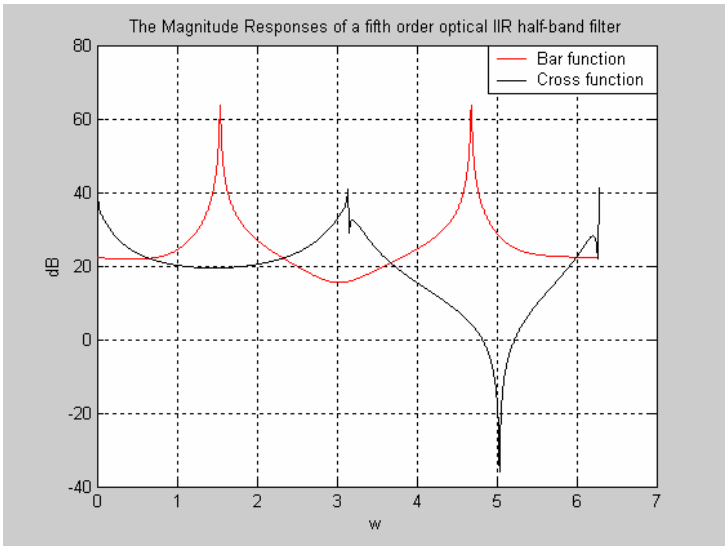

Figure 32: The Magnitude Response of the transfer functions of the bar and the cross functions of the fifth order optical IIR HBF.

2.6 Design of the real fifth order IIR half-band low-pass filter

In this section, the design technique for a real optical fifth order IIR elliptic HBF. In order to design the optical real HBFs (elliptic typed-filter), Miltra [35] implemented the design procedure in which four steps in order need to carry out. The optical odd-order elliptic IIR (low-pass) HBF is designed first by choosing the pass-band edge frequency, say 0.4π. Hence, the corresponding stop-band edge frequency is calculated by $\omega_s = \pi - \omega_p = \pi - 0.4\pi = 0.6\pi$ which can be accepted as for low-pass filters stop-band edge frequency has to be larger than its pass-band edge frequency. *Figure 33* shows the pole-zero plot of the optical fifth-order elliptic half-band low-pass filter as follows.

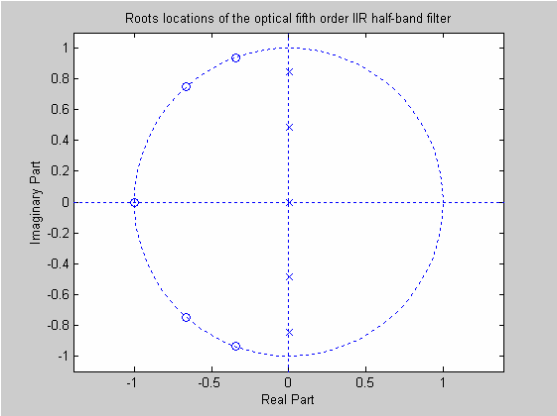

Figure 33: The Roots locations of the real fifth order optical IIR half-band low-pass filter.

Poles	Zeros
0.0007 + j0.8455	-1
0.0007 – j0.8455	-0.3457 + j0.9383
0.0005 + j0.4866	-0.3457 – j0.9383
0.0005 – j0.4866	-0.6626 + j0.749
0.0005	-0.6626 – j0.749

Table 9: Poles and zeros locations of the real fifth order optical IIR half-band low-pass filter.

Although *Figure 33* shows that all poles lay on the imaginary axis in the z-plane, ***Table 1****Table 9*above shows that not exactly on the imaginary axis. However, they are much closed to and the differences are quite small which is due to the fourth decimal, they can be ignored. Thus, they can be considered that the poles are at z = ± j0.8455, z = ± j0.4866, and z = 0.

The frequency responses are illustrated in *Figure 34* and *Figure 35* below.

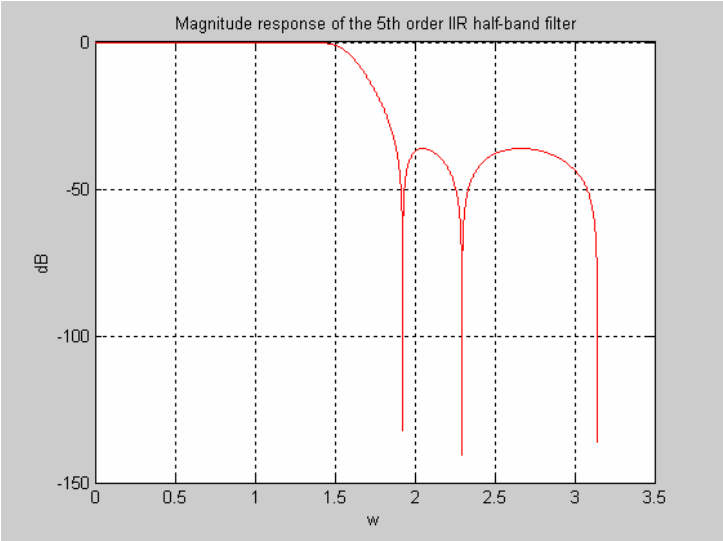

Figure 34: The Magnitude Response of the real fifth order optical IIR half-band low-pass filter.

For the sharp filters, the stop-band attenuation is much greater than the pass-band attenuation. If the minimum order of the optical elliptic IIR HBF is 5, the stop-band attenuation can be chosen about 40dB that means 0.01. And the pas-band attenuation or ripple is related to the stop-band ripple by $\delta_s^{\,2} = 4\delta_p\left(1-\delta_p\right) = 0.25\times 10^{-4}$.

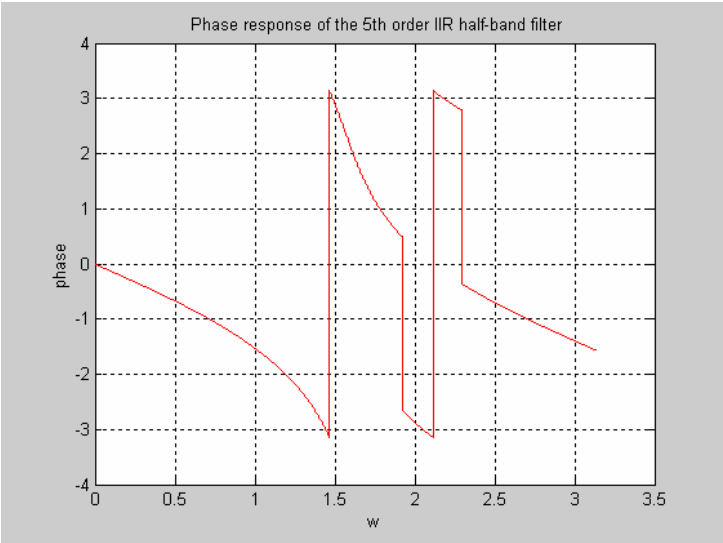

Figure 35: The Phase Response of the real fifth order optical IIR half-band low-pass filter.

This optical fifth order IIR HBF can be re-written as the sum of two all-pass functions.

$$G(z) = \frac{1}{2}\left[A_1(z^2) + z^{-1}(z^2)\right] \quad \text{Eq. 53}$$

If all-pass function A1(z^2) is consisted of poles z = 0 and z = ± j0.4866, and the poles at z = ± j0.8455 is formed all-pass function A2(z^2), the transfer function of the optical fifth order IIR HBF can be represented as

$$A_1(z^2) = \frac{z^{-2} + 0.2368}{1 + 0.2368z^{-2}} \quad \text{Eq. 54}$$

$$A_2(z^2) = \frac{z^{-2} + 0.7149}{1 + 0.7149z^{-2}} \quad \text{Eq. 55}$$

It is the fact that $A_1(z^2)$ is an even function of z while z^{-1} $A_2(z^2)$ is an odd function of z. Thus in the time domain the even-indexed samples of the impulse response g[n] come from the first all-pass function, whereas the odd-indexed samples come from the second all-pass function. This "even-odd" decomposition may be shown to be a consequence of the half-band property [**35**], [**36**].

So, if it is the case for the complex HBF, as stated in Equation 3.26, the complex HBF H(z) is obtained as follows.

$$H(z) \cong 2G(-jz) = \left[A_1(-z^2) + jz^{-1}A_2(-z^{-2})\right] \quad \text{Eq. 56}$$

$$where \begin{cases} A_1(z^2) = \dfrac{z^{-2} + 0.2368}{1 + 0.2368z^{-2}} \\ A_2(z^2) = \dfrac{z^{-2} + 0.7149}{1 + 0.7149z^{-2}} \end{cases} \quad \text{Eq. 57}$$

In this section, the case studies of optical FIR HBFs and IIR HBFs are investigated. Their circuit configurations [**14**] consist of 2 × 2 directional couplers with different path length differences and optical phase shifts.

Optical FIR HBFs are described as a class of optical HBFs where the location of the poles are at the origin of the unit circle which are formed by only feed-forward waveguides and their impulse responses are limited in finite time. In fact, figure 6.1 illustrates the circuit configurations of the

optical FIR HBFs whose consist of (N-1) MZI's with a difference path length of 2ΔL and one MZI with a single path length difference of ΔL. Thus, there are two ways to design the circuit where one configuration has the MZI with single path length difference ΔL on the input-port side and the other on the out-put side. Hence, they can be transformed into each other by reversing their input and output ports. Their transfer functions of the bar and the cross functions are computed by the power ratio between the same input light-wave port of the first coupler and two output light-wave ports of the last coupler. Thus, the condition for realizing optical FIR HBFs is to meet the required power half-band property. For the case of length-2 type, the magnitude responses of the corresponding transfer functions of the bar and the cross functions conserve the total optical energy. For instance, in the range form 3 to 4.5 radians, when the magnitude response of the bar function pulls up, that of the cross function pulls down. As the results of their magnitude responses, because there is no affect of the poles either the cross or bar functions can be chosen in order to capture the properties of the optical FIR HBFs.

In the other hands, optical IIR filters consist of feed-back loops such as ring-waveguides, the location of the poles are within the unit circle to just satisfy the stability of such systems, and their impulse responses are continue for infinite time. The example of optical fifth order IIR HBF and its magnitude response that is shown in *Figure 31* describes that the required half-band property is met and as the affect of the poles and zeros, the transfer function of the cross function gives the sharper magnitude response.

In the last section of this paper, the design of the optical elliptic fifth order IIR half-band low-pass filter is described using the design technique. The design shows that this optical HBF is the sum of the two all-pass functions ($A_1(z)$ and $A_2(z)$)

3 Conclusions and Future Works

In this paper, the design techniques and algorithms of photonics filters using optical resonators are described via their transfer functions' characteristics that are yielded directly from the SFG

representation and the Manson's Gain Rule. This SFG method is actually more powerful than the matrix formalism since it not only provides the fast transfer function regarding to the actual flow graph but also describes the relationship between the system stability (the locations of the poles and zeros) and the energy stored in that systems. This graphical technique for obtaining the transfer functions of the optical directional couplers is therefore used to analyze and realize the circuit configurations of the optical band-pass filters and optical HBFs.

The synthesizing process of the two basic optical band-pass filters in Butterworth and Chebyshev types are described under the given set of specifications. In this thesis, two types of realizations are illustrated: the cascaded realization and the parallel realization. They consist of number of APOC (All Pole Optical Circuits), AZOC (All Zero Optical Circuits) and SPSZR (Single-pole Single-zero Optical Resonators). With the Cascading Realization, by using the locations of poles and zeros that had been computed in the Optical Specifications and Synthesis Algorithms, the numbers of subsystems will be provided and the Tandem Block Diagram [27] will be drawn in order to express how the design would be implement. In the other hands, the Parallel Realization, after the new form of transfer function had been computed; the Parallel Block Diagram [27] that has the number of basic elements is the number of subsystems would be drawn. In order to achieve the same specifications, the Chebyshev optical band-pass filters with lower order which leads to the less number of optical resonators are required and because of the ripple affect, the Chebyshev type proves its better performance against the Butterworth type. It is noted that the 4-port optical directional couplers are used to generate the APOCs and AZOCs while the 6-port optical directional couplers are used to form the SPSZORs. The APOCs and AZOCs are designed to consist of number of poles with corresponding zeros at the origin and numbers of zeros with corresponding poles at the origin respectively. Thus, when they are in the same order they could be cascaded so that all of poles and zeros that appeared at the origin could be cancelled each other. While the pair of single-pole and single-zero can be designed by a 6-port optical directional coupler. Thus, combining multiple-port optical couplers, particularly 4-port

and 6-port optical couplers together did give more flexible methods to design a same desired filter. Furthermore, the multiple-port optical couplers are also the technique that allows having multiple input-output ports and saving optical devices since they would use the same common intersection. However, because this technique to realize the OFs under the given set of specifications is varying and choosing the optical coefficients such as optical phase shifts, intensity transmission coefficients, and intensity coupling coefficients; the hardware implements are very tough to achieve the exact values of these optical coefficients. A part from that, the advantage of this technique is the flexible to choose the optical coefficients and the type of realization methods.

Furthermore, the filtering affects of these 8^{th} order and 6^{th} order Butterworth and Chebyshev optical band-pass filters over the 40 Gbps/channel optical signals modulated with various modulation formats such as DSB, VSB CS-RZ are described as the second goal of this thesis. It is because a higher bit rate of 40 Gbit/s has the advantages over the commercial 10 Gbit/s systems such as an increase in spectra efficiency and a significant reduction in the number of channels for the same capacity. It is known that the VSB (Vestigial Sideband) had been proved to have an advantage against DSB (Double Sideband) in bandwidths' point of view. In fact, by eliminating the redundant spectral components of DSB signals, VSB modulation format can enhance the spectral efficiency roughly by 40%. Further, the characteristics of the CS-RZ (Carrier-suppressed Return-to-Zero) format is more attractive since it could allow higher input power than the conventional RZ format due to the fact that the phase of neighbouring pulses differs by 180^0 phase shift, the interaction between them is suppressed. The high spectral efficiency of the combination of VSB CS-RZ format is considered as the promised solution that suit for high channel bit rate 40 Gb/s. As the increasing number of DWDM systems, group velocity dispersion is required for high transmission rates. Thus, at 40 Gbps/channel, networks are very sensitive to dispersion, so there is an essential need for a system that can be carried into the field to take a quick measurement of the dispersion. With the lower order and much lower

pass-band bandwidth, Chebyshev Band-pass OF did show its potential again that of the Butterworth. The conclusion is that the VSB CS-RZ is the most suitable modulation format for filtering in terms of bandwidth, distortion, spectral efficiency. Although there was still distortion even in the case of Chebyshev filter, the advantages of VSB over DSB had clearly been seen as that for VSB CS-RZ, the bandwidth at -30dB is observed at nearly 80 GHz while DSB CS-RZ reaches approximately 180 GHz which is more than twice that of VSB CS-RZ can achieve. In this section, the bit error rate factor needs to improve as it just reaches 10^{-12} (say it needs to achieve at least 10^{-9}). This kind of improvement might be done by applying the better type of OF such as elliptic OF to achieve the ripple affects, lower order, less distortion (BER), and so on.

Further, the potential applications of the multi-rate digital signal processing systems to achieve different sampling rates at different stages is described via the characteristics of optical HBFs. Here, the optical HBF is defined as the term generally used to describe special filters that are suitable for the rate conversion by a factor of two. The case studies of optical FIR HBFs and IIR HBFs are described. In both cases, the energy stored in the systems as well as the required power half-band property are confirmed by studying the characteristics of the transfer functions of their bar and the cross functions. As the results of the magnitude responses, because there is no affect of the poles either the cross or bar functions can be chosen in order to capture the properties of the optical FIR HBFs. While the frequency responses of the cross function of the fifth order IIR HBF has the advantage against that of the bar function. Finally, the case of the real optical elliptic fifth order IIR half-band low-pass filter is described. It is illustrated as the sum of two all-pass functions which can realize as a complex HBF if the real and the imaginary parts are taken separately. The frequency responses show the short transition from pass-band to stop-band which causes by the location of the zeros near the unit circle. In this thesis, only the cases that are derived from the odd-ordered recursive HBFs are concerned. These odd-ordered characteristics are composed by two all-pass functions $A_1(z)$ and $A_2(z)$. However, it is similar to design the

even-ordered type by just substituting the transfer function of $A_2(z)$ by its complex conjugate [36].

4 References

[1] J. Hecht, "Understanding Fiber Optics," 2002.
[2] Y. N. Chew, T. T. Tjhung, and F. V. C. Mendis, "Performance of single and double-ring resonators," *J. Lightwave Technol.*, vol. 11, pp. 1998-2008, 1993.
[3] P. A. Davies and G. Abd - El – Hamid, "Four-port fiber-optic ring resonators," *Electron. Lett.,* vol. 24, no. 11, pp. 662-663, 1998.
[4] P. A. Davies and G. Abd - El – Hamid, "Four-port fiber-optic double ring resonators," *Electron. Lett.,* vol. 25, no. 3, pp. 224-225, 1989.
[5] L. J. Cimini, Jr., L. J. Greenstein, and A. A. M. Saleh, "Optical equalization for high-bit-rate fiber-optic communications," *IEEE Photon. Technol. Lett.,* vol. 2, pp. 200-202, 1990.
[6] L. J. Cimini, Jr., L. J. Greenstein, A. H. Gnauck, and L. W. Stulz, "Optical equalization of fiber chromatic dispersion of a 5-Gbps transmission systems," *IEEE Photon. Technol. Lett.,* vol. 2, pp. 585-587, 1990.
[7] L. F. Stokes, M. Chodorow, and H. J. Shaw, "All single mode fiber resonators," *Opt. Lett*., vol. 7, pp. 288-290, 1982.
[8] F.Zhang and J. W. Y. Lit, "Direct-coupling single-mode fiber ring resonators," *J. Opt. Soc. Am. A,* vol. 5, no. 8, pp. 1347-1355, 1988.
[9] L. N. Binh, Shu Fun Luk, and N. Q. Ngo, "Graphical Representation and Analysis of the Z-shaped double-coupler optical resonator," *J. Lightwave Technol.*, vol. 11, no. 11, pp. 1782-1792, 1993.
[10] L. N. Binh, N. X. Thien, and N. Q. Ngo, "Realization of Butterworth-type OFs using 3 × 3 coupler ring resonators," *IEE Proc.-Opt.,* vol. 143, no. 2, pp.126-134, 1996.
[11] T. Tsuritani, A. Agata, K. Tanaka, N. Edagawa, and I. Morita, "Performance comparison between DSB and VSB signals in 20Gbps-based ultra-long-haul WDM systems," *ECOC2000*, 2000.
[12] D. Breuer and K. Petermann, "Comparison of NRZ and RZ modulation formats for 40Gbps TDM standard-fiber systems," *IEEE Photon. Technol. Lett.,* vol. 9, pp. 398-400, 1997.
[13] Y. Zhu, W. S. Lee, P. Lobb, C. Ward, D. Watley, S. Savory, C. R. S. Fludger, B. Shaw, and A. Hadjifotiou, " Polarization-channel-interleaved CS-RZ transmission at 40Gbps with 0.8bit/s/Hz spectral efficiency," *Electron. Lett.,* vol. 38, no. 8, pp. 381-382, 2002.
[14] K. Jinguji and M. Oguma, "Optical HBFs," *J. Lightwave Technol.*, vol. 18, no. 2, pp. 225-259, 2000.
[15] P. P. Vaidynathan and T. Q. Nguyen, "A trick for the design of FIR HBFs," *IEEE Trans. Circuits Syst.,* vol. CAS-34, pp. 297-300, 1987.
[16] John R. Ward and Robert D. Strum, "The SFG in Linear Systems Analysis (A programmed text),"
[17] V. D. Vegte, "Feedback control systems,"
[18] "Electronic circuits – Discrete and integrated,"
[19] E. W. Kamen and B. S. Heck, "Fundamentals of signals and systems," *Prentice Hall,* Upper Saddle River, N. J., 1997.
[20] X. Zhang and K. Amaratunga, "Closed-form design of Maximally flat IIR HBFs," *IEEE Trans. Circuits Syst.,* vol.49, no. 6, pp. 409-410, 2002.
[21] N. Q. Ngo, "New optical signal processors: Design and application to optical computing and optical communication systems," *Thesis*, pp. 26-31, 1997.
[22] S. J. Manson, "Feedback theory-some properties of SFGs," *Pro. IRE*, vol. 41, pp. 1144-1156, 1953.

[23] S. J. Manson, “Feedback theory-further properties of SFGs,” *Pro. IRE*, vol. 44, pp. 920-926, 1956.
[24] J. J. Distefano, A. R. Stubberub, and I. J. Williams, “Theory and problems of feedback and control systems,” *McGraw-Hill*, ch. 8, 1987.
[25] J. Stone and C. A. Burrus, “Neodymium doped silica lasers in end-pumped fiber geometry,” *Appl. Phys. Lett*., vol. 23, pp. 388, 1973.
[26] P. Urquhart, “Fiber lasers with loop reflectors,” *Appl. Opt.,* vol. 28, pp. 3759, 1989.
[27] L. N. Binh, “Synthesis of optical band-pass Chebyshev filters,” 2003.
[28] R. W. C. Vance, “Planar ring resonator realization of symmetric 3 × 3 fiber coupler,” *Electron. Lett.,* vol. 30, no. 15, pp. 1222-1223, 1994.
[29] T.Tsuritani, and Akira Agata, et al, “35GHz-spaced-20 Gbps-based 100 WDM RZ transmissions over 2700 km 2000 using SMF based dispersion flattened fiber span,” *ECOC 2000*, PD 1.5, 2000.
[30] T.Tsuritani, I. Morita, and A. Agata, “Ultra long-haul transmission with multi-terabit capacity,” *ECOC 2001*, PD 1.5, 2001.
[31] S. Bigo, “5.12 Tbit/s (128 × 40 Gbit/s WDM) transmission over 3 × 100km of Tera-light fiber,” *ECOC 2000*, PD 1.2, 2000.
[32] T.Tsuritani, “1 Tbit/s (10 × 10.7 Gbit/s) transoceanic transmission using 30 nm wide broadband optical repeaters with Aeff-enlarged positive dispersion fiber and slope-compensating DCF,” *Electron. Lett.,* vol. 35, pp. 2126-2128, 1999.
[33] A. Sano, and Y. Miyamoto, “Performance Evaluation of Prechirped RZ and CS-RZ formats in high-speed transmission systems with dispersion management,” *J. Lightwave Technol.*, vol. 19, no. 12, pp. 1864-1867, 2001.
[34] H. J. Orchard and G. C. Temes, “Design technique for Vestigial-sideband filters,” *Trans. Comm. Syst.,* vol. COM-22, no. 7, pp. 956-957, 1974.
[35] S. K. Mitra, “Digital Signal Processing: A computer-based approach,” *The McGraw-Hill Companies, Inc.*, pp. 697, 1998.
[36] S. K. Mitra and J. F. Kaiser, “Handbook of Digital Signal Processing,” *J. Wiley & Sons*, pp. 909-1013, 1993.